Section 3
Statistical Accident Scenario Analysis and CASRAM

CASRAM is a quantitative risk assessment model for analyzing hazardous material transportation accidents. This model lies at the core of the 2000ERG analysis. It predicts distributions of hazard zones (i.e., areas in which a threshold chemical concentration is exceeded) and distributions of affected populations as a result of releases associated with hazardous material transportation or storage. The model uses various shipment attributes together with an extensive meteorological database to statistically generate and analyze hazardous material release scenarios. For a given health end-point (i.e., toxicological threshold concentration), distributions of hazard zones are generated stochastically through Monte Carlo sampling of accident scenario parameters (e.g., time, location, release amount, meteorology) and detailed consequence modeling of the hypothetical releases. CASRAM is specifically designed for the *statistical* analysis of hazardous material release problems. This feature, in particular, separates CASRAM from many other hazardous material release models. Rather than specifying a deterministic measure of risk, CASRAM determines the distribution of possible outcomes, thus allowing identification of the probability of a particular consequence within the limits of the statistical data.

CASRAM is primarily a routing-based risk assessment model that requires shipment attributes (e.g., materials, containers) and shipment routes as inputs. It provides distributions of affected persons as outputs (e.g., Brown et al. 1999). However, it is equally applicable to a geographically based incident distribution system. A geographically based system is required for the ERG analysis because the Table must reflect releases that occur anywhere in North America. The statistical accident scenario analysis (see Figure 2.1) combines the shipment profile information discussed in Section 2.2, meteorological observations from a preprocessed meteorological database, and statistical information from the HMIS database to provide a large distribution of incidents. These incidents are then modeled by using the consequence models within CASRAM. The overall goal of this analysis is to identify the distributions of safe distance (i.e., hazard zone length) associated with the transport within North America of all materials that are given in the Table. The Protective Action and Initial Isolation Distances in the Table are the 90-percentile values of these safe-distance distributions.

This section first discusses the statistical scenario analysis and then the meteorological database used in the 2000ERG study. The emission rate modeling and dispersion modeling within CASRAM, which make up the consequence modeling effort to determine PADs, are then outlined.

3.1 Statistical Scenario Analysis

3.1.1 Overview of Analysis Steps

For each material in the Table, CASRAM was used to model between 40,000 and 100,000 separate incidents. For this analysis, incidents were distributed among different transportation modes (e.g., highway, rail), container types (e.g., DOT class 105 tank car, MC 330 cargo tank), and release types (e.g., accident-related, en route/nonaccident) specified in the shipment profile. Examples of incident distributions among these release categories are provided in Section 2.2.1. Incidents were also distributed geographically and temporally on the basis of transportation mode and release type. Geographic and temporal effects have a large influence on meteorology, which in turn directly affects the safe distance calculation. The location of the incident affects the general climate and land use (e.g., dry desert, temperate farmland), whereas the time of day and month affect the weather at that locale.

Each release modeled in the analysis is assigned a random date, time, and location. The locations for U.S.-based accidents are chosen probabilistically on the basis of state distributions of accidents in the HMIS database. Separate distributions are used for accident-related and en route/nonaccident releases for both highway and rail. Locations for Canada and Mexico are based on population density. Date and time are assigned on the basis of month-of-year and time-of-day distributions for incidents in the HMIS database following Brown et al. (1999), where the year is assigned in a five-year window that corresponds to observations in the meteorological database (1985–1989).

The emission rate model in CASRAM uses the shipment information and meteorology as specified above to determine the rate at which specific materials are released into the atmosphere. The first step is to estimate the discharge fraction on the basis of historical statistical distributions generated from analysis of HMIS database incidents. The emission rates of the material to the atmosphere are then calculated by using physical models for discharge, flashing, and evaporation applicable to that release. Within the emission rate model, the total amount of material spilled (discharge fraction) and pool size are treated stochastically.

By using the emission rates for the chemical(s) involved and the ambient meteorology, the dispersion model within CASRAM then determines the affected areas. Calculation of dispersion in CASRAM is basically a two-step process. Step 1 involves characterizing the meteorology from the available surface observations. Step 2 involves estimating the transport and dispersion from the applicable meteorological parameters. Step 1 is accomplished with a *meteorological preprocessor*, which consists of a series of algorithms that take raw meteorological data (e.g., wind speed, temperature, humidity, cloud cover) and site information (e.g., land cover type, roughness length) and calculate parameters necessary for estimating dispersion. While this analysis is usually closely associated with dispersion modeling, the atmospheric parameters calculated are also used in estimating source emission rates. Traditionally, these parameters have been represented as stability classes; however, in this analysis, the turbulence of the

atmospheric boundary layer was represented by more fundamental turbulence measures, such as friction velocity, surface heat flux, and inversion height. Step 2 is accomplished by using a Lagrangian integral dispersion model for passive releases, coupled with a dense gas dispersion model to address large releases of liquefied gases where heavier-than-air plumes form. The physical relationships that makeup the emission rate and dispersion models are outlined in Sections 3.3 and 3.4, respectively.

3.1.2 Key Statistical Data Employed

3.1.2.1 Geographic Incident Distributions

In the 2000ERG analysis, accidents are distributed across all 50 states in the United States, the southern Canadian provinces, and Mexico. Within the United States, the accident distribution is based on incident distributions in the HMIS database for 1985 through 1995, and separate geographic distributions are used for highway and rail. The distribution of accidents among the United States, Canada, and Mexico is based on the total gross domestic product (GDP) for 1997. The total GDP was selected as a measure for hazardous materials incidents because detailed data on these incidents in Canada and Mexico are not available. For the United States and Canada, the relative GDP for chemical and chemical products is similar to the total GDP, but because the industry-specific GDP was not available for Mexico, and because Canadian and U.S. chemical-specific GDPs are calculated slightly differently, the total GDP was considered to be the more robust indicator. On the basis of this breakdown, 89% of incidents modeled in the 2000ERG analysis occurred in the United States, 7% occurred in Canada, and 4% occurred in Mexico. Within Canada and Mexico, incidents were distributed into regions on the basis of population. Canada was divided by province. In this process, New Brunswick, Newfoundland, Nova Scotia, and Prince Edward Island were combined as the "Atlantic Provinces," and the Yukon and Northwest Territories were excluded because of their small populations (more than 0.5% of total Canadian population). Mexico was divided into three regions: Northern (above 22°N latitude), Central (between 18 and 22°N latitude), and Southern (below 18°N latitude, including the Yucatan Peninsula). A breakdown of the geographic distribution of incidents in the 2000ERG analysis for highway and rail transportation is provided in Table 3.1.

3.1.2.2 Temporal Incident Distributions

Temporal release distributions are important in determining meteorology. In some risk assessment studies, temporal variables also influence the population at risk because the number of people at a particular location may change throughout the day and because more people may be outside during the day. Two temporal variables are defined in the analysis: hour of day and day (or month) of year. With regard to meteorology, the hour of day is critical because of the diurnal cycle of the atmospheric boundary layer, and the day of year is important because of seasonal effects on wind speed, temperature, cloud cover, and daytime mixing height. Note that wind speed and temperature affect not only dispersion but also the emission rate of spilled liquids to the atmosphere.

Table 3.1 Geographic Distribution of Highway and Rail Transportation Incidents Modeled in the 2000ERG Analysis, by Percentage

State/Province	Highway	Rail	State/Province	Highway	Rail
Alabama	1.85	2.76	New Mexico	1.45	0.68
Alaska	0.12	0.40	New York	2.61	1.10
Arizona	1.51	0.88	North Carolina	2.42	2.33
Arkansas	2.56	3.33	North Dakota	0.22	0.12
California	4.62	8.62	Ohio	6.10	4.93
Colorado	1.60	1.21	Oklahoma	1.30	0.95
Connecticut	0.79	0.04	Oregon	1.22	1.55
District of Columbia	0.04	0.00	Pennsylvania	6.51	1.82
Delaware	0.26	0.12	Rhode Island	0.18	0.03
Florida	2.02	1.83	South Carolina	1.09	0.74
Georgia	2.43	2.91	South Dakota	0.18	0.00
Hawaii	0.02	0.00	Tennessee	3.20	1.94
Idaho	0.46	1.00	Texas	6.98	11.54
Illinois	5.54	5.40	Utah	0.94	1.97
Indiana	2.49	1.74	Vermont	0.16	0.01
Iowa	1.27	0.63	Virginia	1.75	1.46
Kansas	1.78	2.34	Washington	1.35	1.54
Kentucky	2.00	1.38	West Virginia	1.08	0.66
Louisiana	3.20	5.52	Wisconsin	1.35	0.23
Massachusetts	1.25	0.21	Wyoming	0.63	2.40
Maryland	1.45	0.64	Canada and Mexico		
Maine	0.28	0.12	British Columbia, Can.	0.82	0.82
Michigan	1.83	3.55	Alberta	0.63	0.63
Minnesota	1.52	0.42	Saskatchewan	0.25	0.25
Mississippi	1.24	0.84	Manitoba	0.27	0.27
Missouri	2.51	2.85	Ontaria	2.51	2.51
Montana	0.33	0.58	Quebec	1.71	1.71
Nebraska	0.63	1.85	Atlantic Provinces	0.58	0.58
Nevada	0.48	0.68	Northern Mexico	1.03	1.03
New Hampshire	0.17	0.00	Central Mexico	2.69	2.69
New Jersey	1.80	0.90	Southern Mexico	0.76	0.76

Temporal incident variations in the 2000ERG analysis are based on statistical data from the HMIS database as presented by Brown et al. (1999) and shown in Figures 3.1–3.4. Temporal distributions are separated by time of day and month of year. The accident rate is assumed to be uniform on a day-of-month basis. The temporal distributions are further delineated by transport mode (highway or rail) and by type of release (accident-related or en route/nonaccident).

3.1.2.3 Discharge Fraction Distributions

In the CASRAM emission model, the discharge fraction is estimated by using statistical distributions developed from an analysis of the HMIS database maintained by

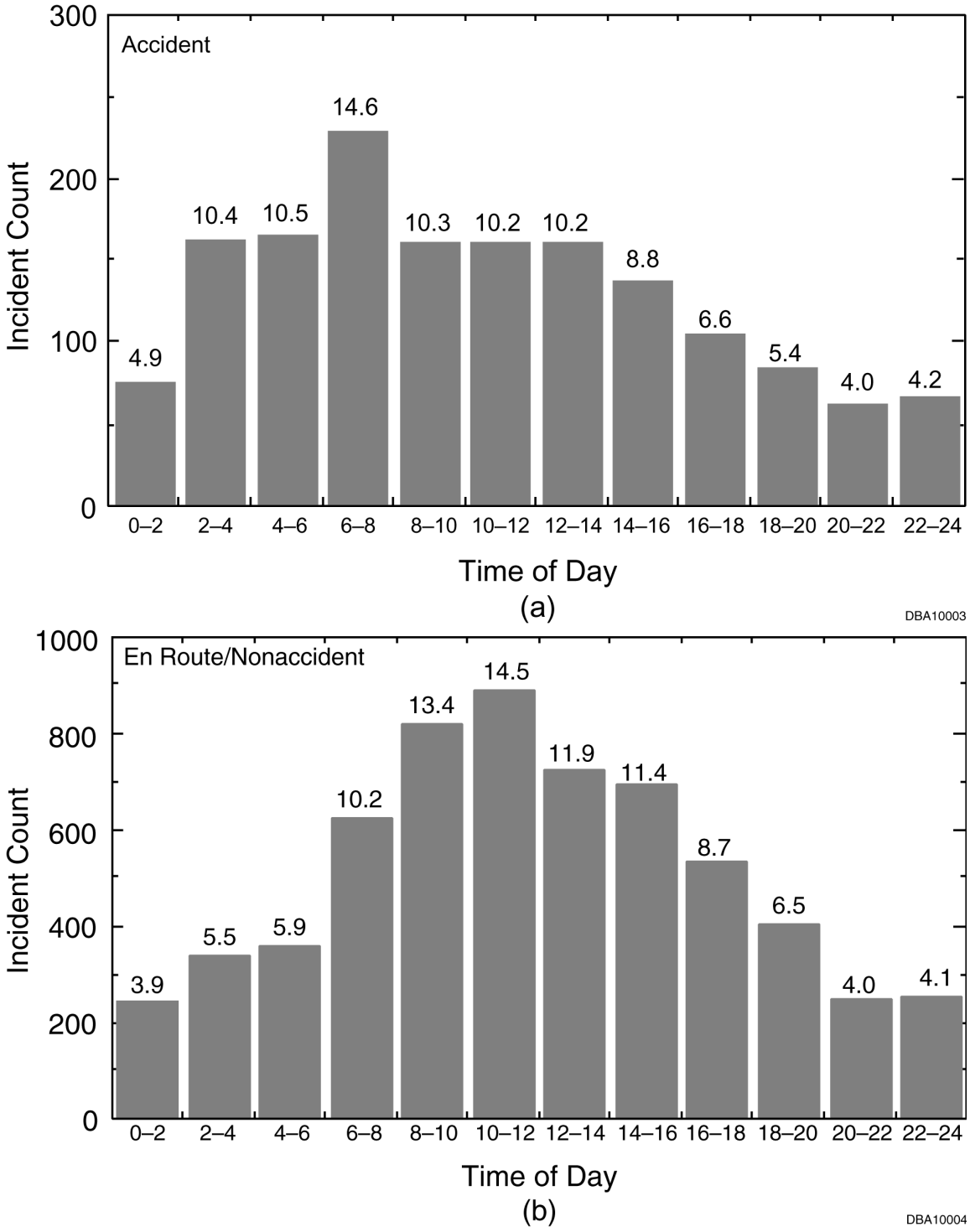

Figure 3.1 Hourly Distribution of Highway-Transportation-Related Hazardous Material Releases (a = releases during vehicle accidents and b = releases during en route/ nonaccident incidents as calculated by Brown et al. [1999] and used in the 2000ERG analysis)

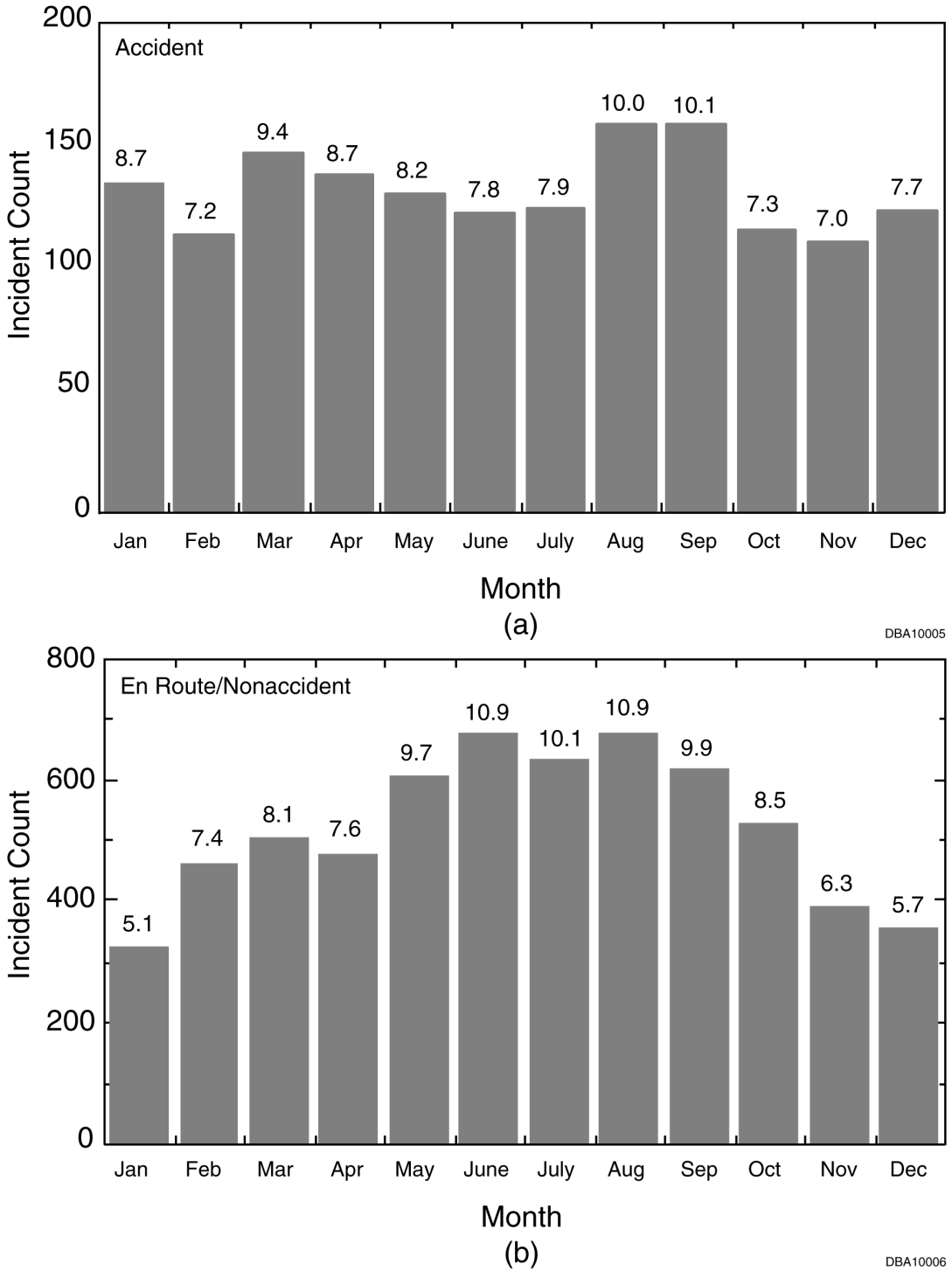

Figure 3.2 Monthly Distribution of Highway-Transportation-Related Hazardous Material Releases (a = releases during vehicle accidents and b = releases during en route/ nonaccident incidents as calculated by Brown et al. [1999] and used in the 2000ERG analysis)

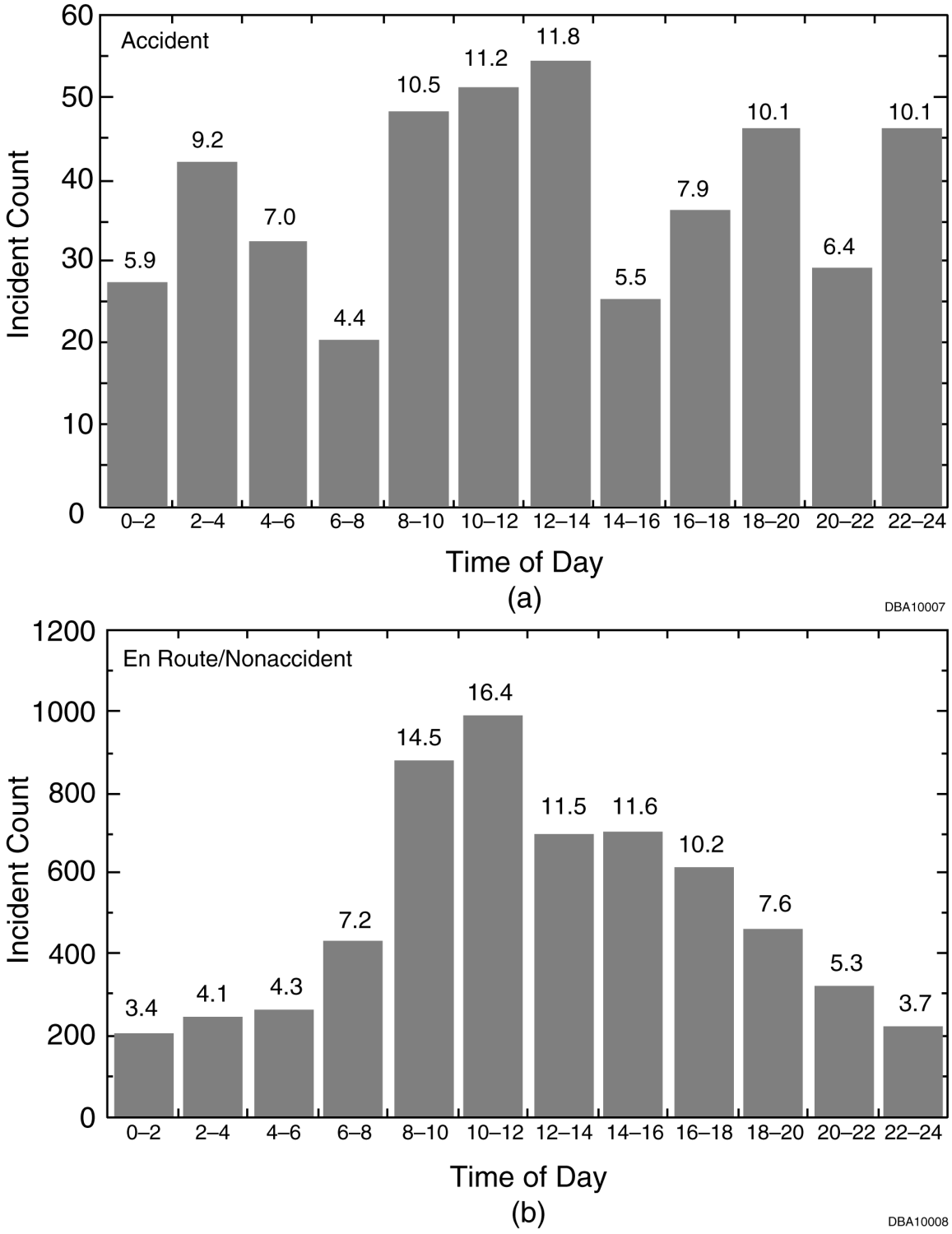

Figure 3.3 Hourly Distribution of Rail-Transportation-Related Hazardous Material Releases (a = releases during vehicle accidents and b = releases during en route/nonaccident incidents as calculated by Brown et al. [1999] and used in the 2000ERG analysis)

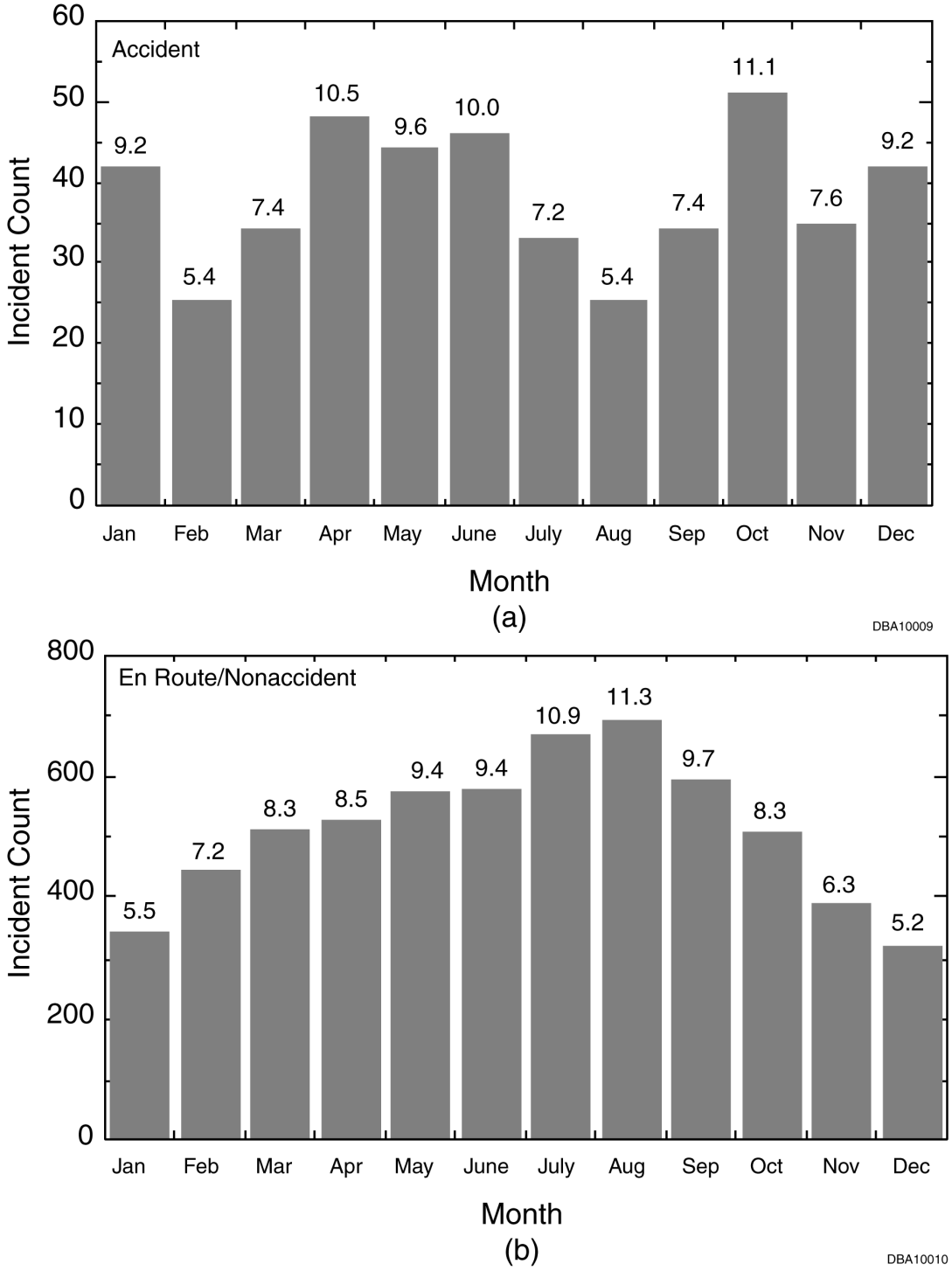

Figure 3.4 Monthly Distribution of Rail-Transportation-Related Hazardous Material Releases (a = releases during vehicle accidents and b = releases during en route/ nonaccident incidents as calculated by Brown et al. [1999] and used in the 2000ERG analysis)

DOT, following the analysis of Brown et al. (1999). The HMIS database consists of coded information collected from U.S. transportation-related incidents involving hazardous materials. It is the best available source of information about container failures and release amounts. For each incident cataloged in the HMIS database, information includes (1) name of chemical shipped, (2) container type, (3) number of containers shipped, (4) number of containers that failed, and (5) amount of material released. In characterizing the amount of a release, the fraction of the container's capacity that was released appears to be the most robust statistic in terms of both aggregating data from a wide variety of containers and ease of use in subsequent risk assessment studies. This fraction of the total container capacity that is released is defined here as the *discharge fraction*. In constructing distributions for the discharge fraction for various container types, the amount that was shipped is inferred by multiplying the number of containers by the container capacity. Since the amount of material actually shipped is not currently provided in the HMIS database, the container capacity provides the best estimate of the amount shipped. As an example, consider a vehicular accident that involves the shipment of four 10-gal drums of acetone and in which 1.6 gal is released. The discharge fraction would be 0.04, i.e., $1.6/(4 \times 10)$. As is discussed later, this incident would be grouped with all other incidents involving drums with capacities of less than 20 gal to construct the discharge fraction distributions for accident-related releases. The discharge fraction for package freight containers involved in en route/ nonaccident releases and in loading and unloading mishaps is calculated on the basis of the capacity of a single container. When the above example is used again, the discharge fraction would be 0.16, i.e., 1.6/10 if the release occurred while en route but not during an accident or during loading or unloading of the drums.

In the CASRAM source model, discharge fraction statistics are segregated according to container type. In general, these container types can be classified according to whether they are used for bulk or package freight. Discharge fraction statistics for bulk containers are shown in Figures 3.5 and 3.6. Figure 3.5 shows discharge fraction distributions for containers that are used for nonpressurized and low-pressure materials. Figure 3.6 shows the distributions for containers that are used for high-pressure materials. Discharge fraction distributions are provided for the two transportation-related phases considered in the ERG2000 analysis: accident-related and en route/nonaccident releases. Discharge fraction statistics for bulk package freight were developed for a specific container type (Type 111A tank cars, MC306 tanks, etc.) when sufficient statistical data were available (i.e., data on at least 25 incidents). In practice, discharge fractions for other container types for which data are insufficient could be estimated by using a surrogate for a similar container type for which data do exist. For example, the surrogate discharge fraction distribution for Type 103 tank cars would be that for Type 111A tank cars, and the surrogate for MC338 cargo tanks would be MC330/331 cargo tanks.

The discharge fraction statistics for accident-related and en route/nonaccident releases for package freight containers and portable tanks are shown in Figure 3.7.

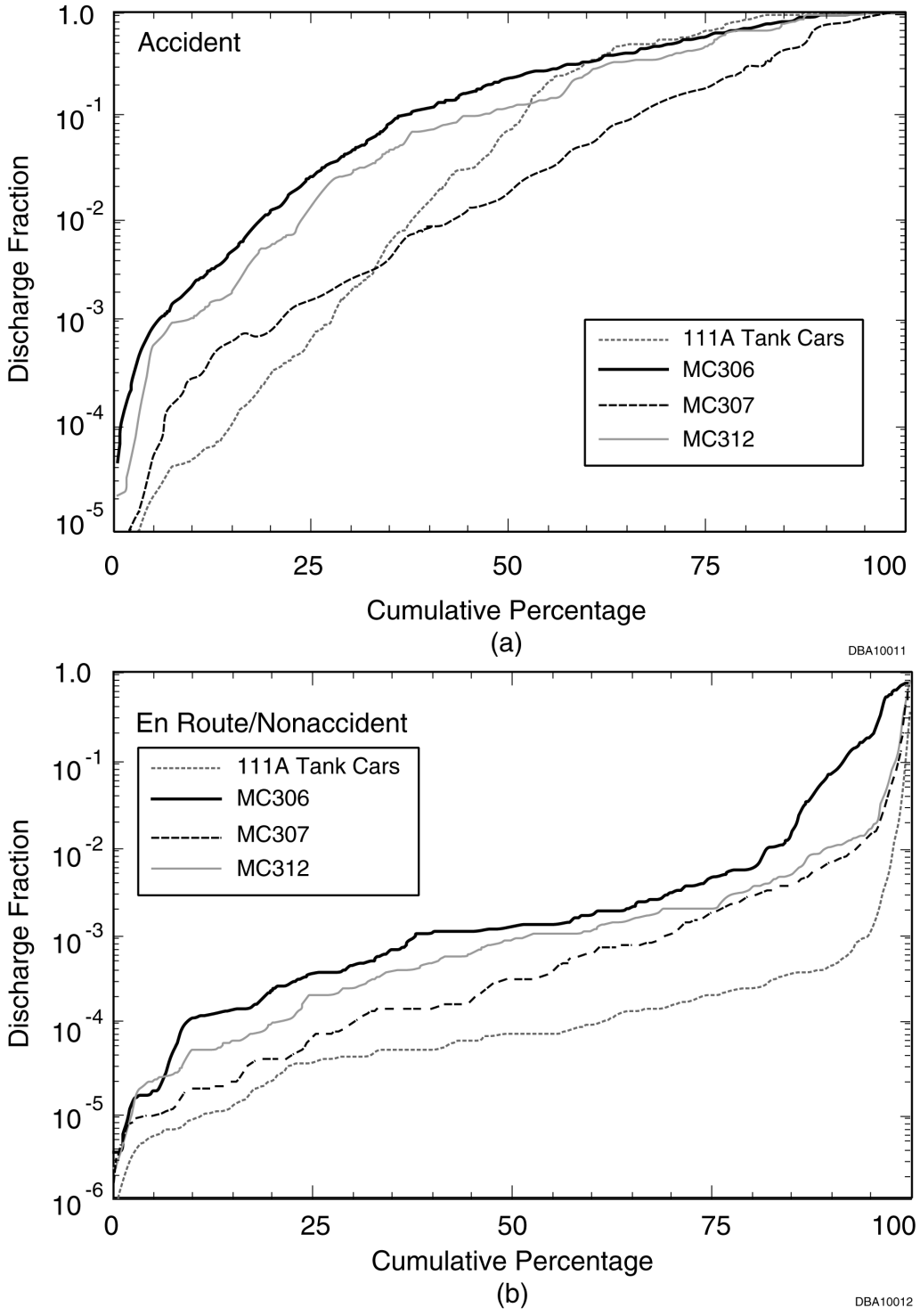

Figure 3.5 Discharge Fraction Cumulative Probability for Bulk Nonpressurized and Low-Pressure Containers as Derived from the HMIS Database (a = accident-related releases and b = en route/nonaccident releases; discharge fraction is fraction of container capacity that was released) (Source: Brown et al. 1999)

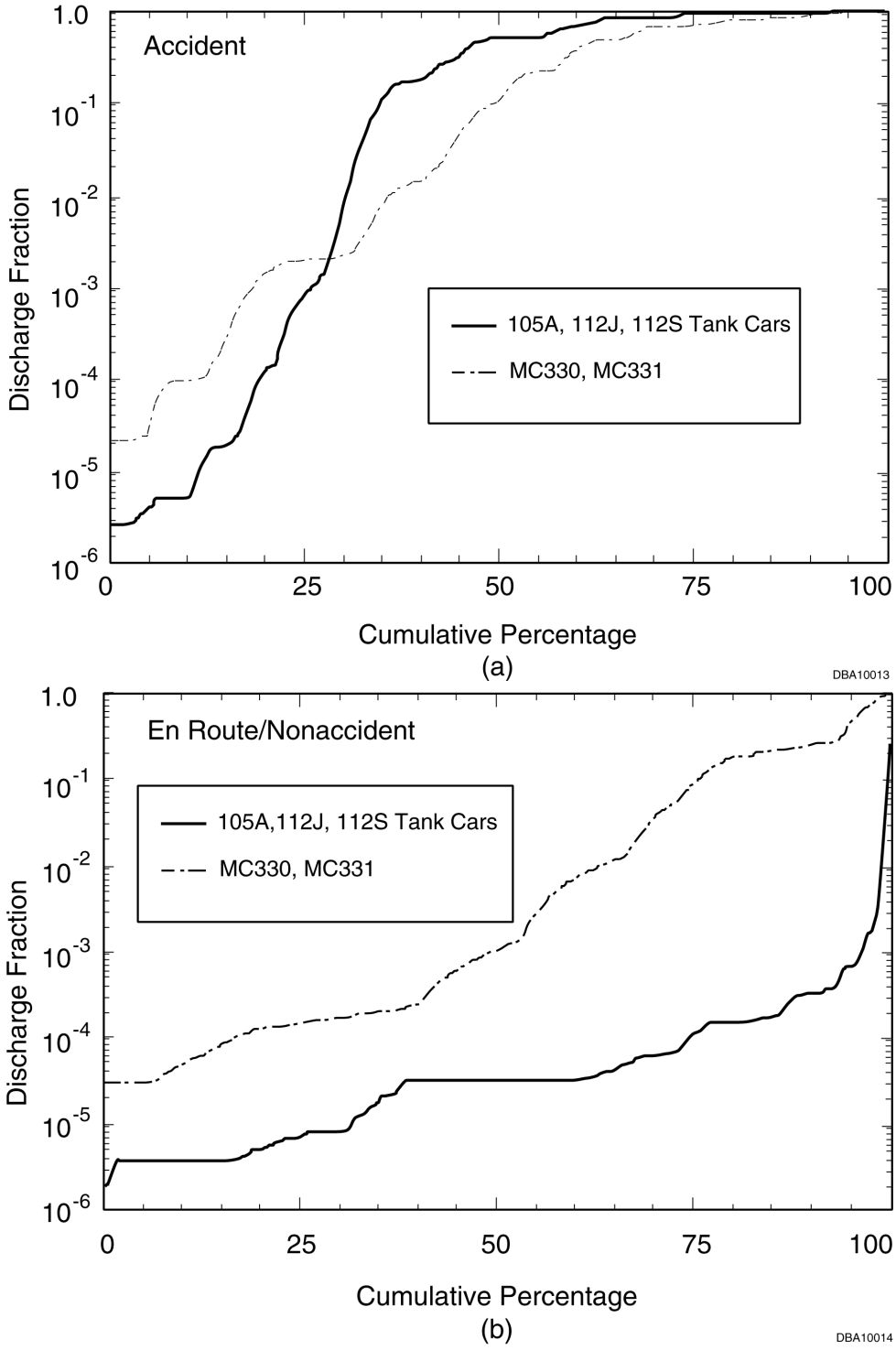

Figure 3.6 Discharge Fraction Cumulative Probability for Bulk Pressurized Containers as Derived from the HMIS Database (a = accident-related releases and b = en route/nonaccident releases; discharge fraction is fraction of container capacity that was released) (Source: Brown et al. 1999)

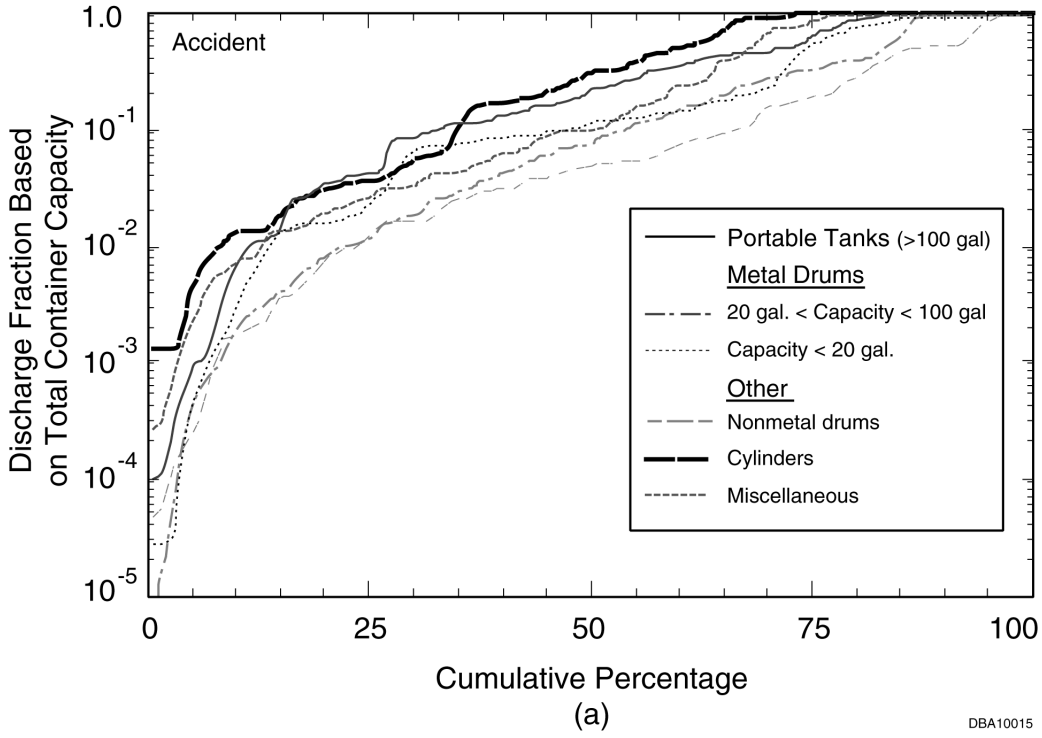

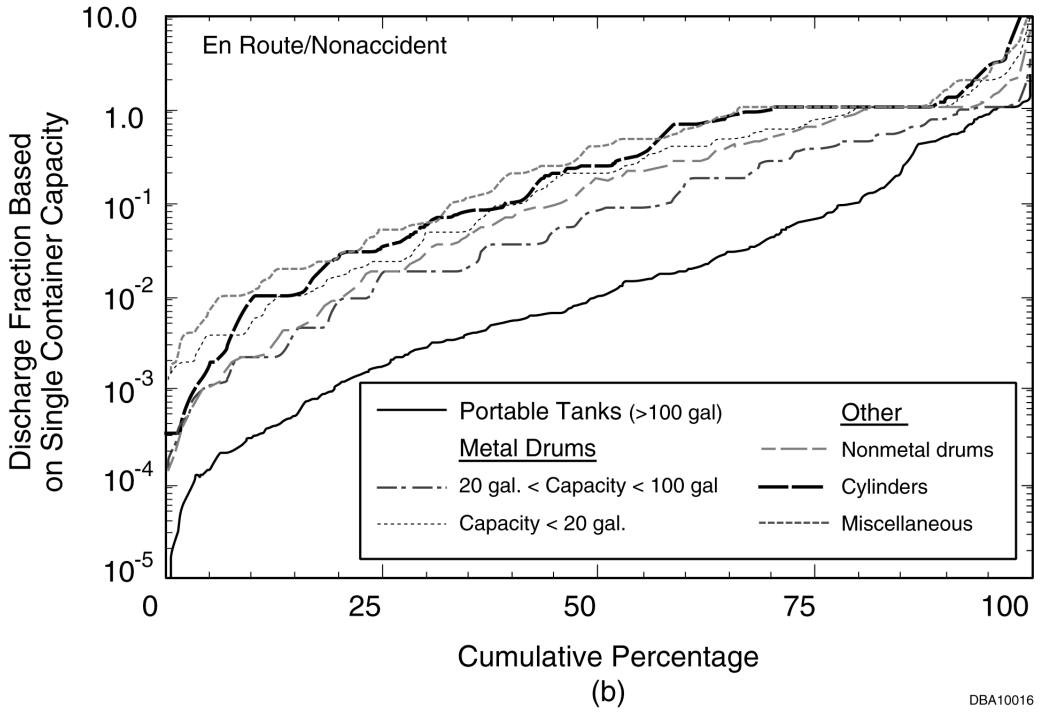

Figure 3.7 Discharge Fraction Cumulative Probability for Package Freight Containers (including portable tanks) as Derived from the HMIS Database (a = accident-related releases and b = en route/nonaccident releases; for a, discharge fraction is fraction of total capacity of all containers that were released; for b, it is fraction of a single container that was released) (Source: Brown et al. 1999)

Because the number of container types was so large, the types were grouped into several categories: (a) portable tanks (including metal drums with capacities greater than 100 gal), (b) metal drums with capacities less than 100 gal but greater than 20 gal, (c) metal drums with capacities of 20 gal or less, (d) nonmetal drums, (e) metal cylinders, and (f) miscellaneous containers. The miscellaneous category includes cans, bottles, pails, jerricans, carboys, and kegs/barrels. The discharge fraction distributions for accident-related releases are given in terms of the amount released as a fraction of the *total container capacity* (i.e., capacity of all containers combined). In contrast, the discharge fraction distributions for en route/nonaccident releases are given in terms of the amount released as a fraction of an *individual container's capacity.* Through trial and error, it was found that this was the most reliable method of scaling discharge fraction statistics over a variety of shipment sizes, since en route/nonaccident releases as well as loading and unloading releases frequently involve damage to only a single container. One drawback of this release fraction normalization is that for a few of the container categories, the distributions do not properly represent shipments that contain only few containers. A method for treating these cases is outlined in Brown et al. (1999).

3.2 Meteorological Database Used to Prepare the Guidebook

The meteorological database is a critical component of the ERG2000 analysis since it provides the historical meteorological data necessary to model hazardous material incidents anywhere in the United States, Canada, and Mexico. This database was generated directly from five years of observational data from 105 cities in the United States and from supplemental data from several stations in Canada and Mexico. The data were first preprocessed by using the Surface Energy Budget Meteorological (SEBMET) model (Brown 1997; Brown and Dunn 1998). This meteorological preprocessor was designed for use with dispersion studies such as the ERG2000 analyses. A meteorological preprocessor contains a series of algorithms that use routinely measured observations of wind speed, temperature, humidity, and cloud cover, along with upper-air temperature soundings, to calculate the key atmospheric-boundary-layer parameters necessary for modeling source thermodynamics, transport, and dispersion. The following sections first discuss the raw meteorological data used in the analysis and then provide a brief overview of SEBMET's methodology. They then describe a companion database employed to estimate water temperature for analysis of water-reactive spills.

3.2.1 Meteorological and Site Data

For the ERG2000 analysis, CASRAM uses a meteorological database that includes hourly meteorological parameters from 105 U.S. cities in 1985 through 1989 (as illustrated in Figure 3.8) and supplemental data from several stations in Canada and Mexico. The stations were chosen to provide a roughly uniform coverage area. Raw meteorological data included yearly surface files listing hourly values of wind speed, temperature, cloud cover (height and fraction), dew point temperature, pressure, and visibility, among other variables. In addition, upper air data from 80 stations across North America were employed to evaluate the atmospheric temperature profile up to the 7,000-m altitude necessary for determining the daytime mixing height. Site

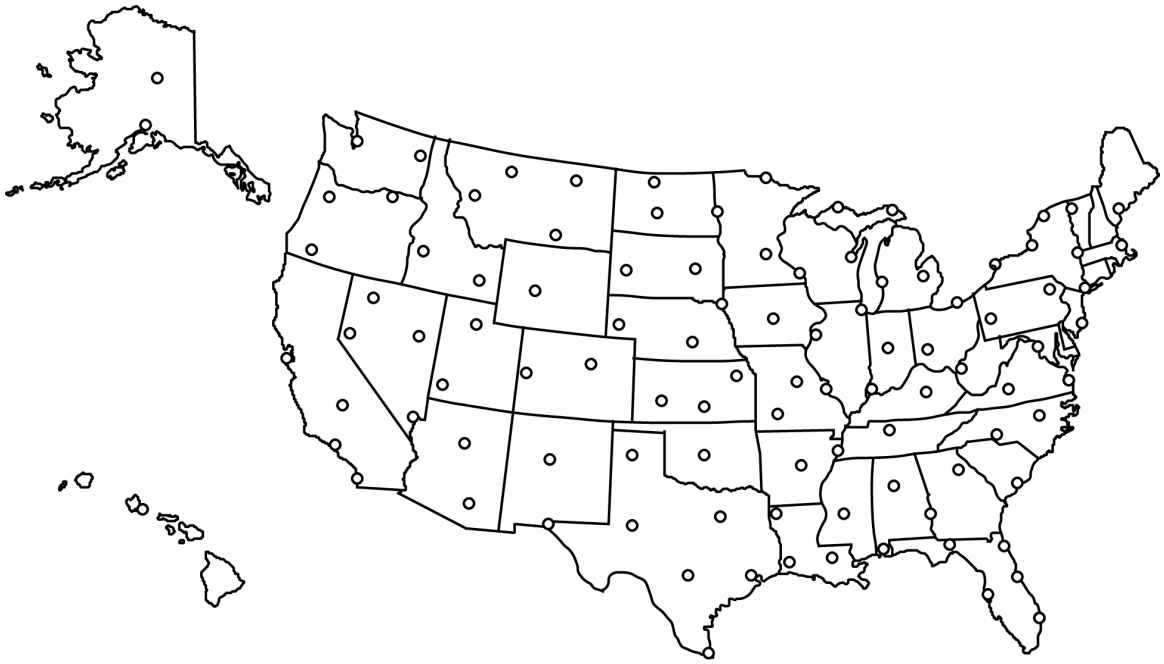

Figure 3.8 Locations of the 105 National Weather Service Stations Used for Statistical Meteorological Characterization

characteristics determined for each station included land cover, vegetative types, the monthly leaf area index (a measure of the canopy density) for each vegetative type, roughness length, albedo, and soil types. These site-specific parameters were determined through a climatological study of the areas surrounding each site.

3.2.2 Meteorological Preprocessor

The meteorological preprocessor contains two primary components: a surface energy budget (SEB) model that determines the surface-layer turbulence parameters and an integral model determines inversion height in convective conditions. Each component is briefly outlined below. Brown (1997) and Brown and Dunn (1998) contain additional information on the meteorological preprocessor, including details on its development and validation.

3.2.2.1 Surface Turbulence Parameters

The surface-layer parameters are determined by using a SEB model that consists of parameterizations of the various SEB components and well-known flux-profile relationships. The goal of this modeling approach is to isolate the sensible heat flux H from the other energy budget components. The starting point for this analysis is the SEB

at the ground. When advection, photosynthesis, and snow melt are neglected, the SEB is most simply represented as follows:

$$Q^* = H + \lambda E_w + G + Q_a, \tag{3.1}$$

where

Q^* = net surface radiative heat flux,

G = conductive soil heat flux,

λ = heat of vaporization for water,

E = evaporation rate (together, λE_w is the latent heat flux), and

Q_a = anthropogenic heat flux.

The net surface radiative heat flux is the residual from the absorbed solar radiation S, incoming long-wave radiation L^+, and outgoing long-wave radiation $\varepsilon\sigma T_S^4$. It is written as follows:

$$Q^* = (1-\alpha_s)\, S + L^+ + \varepsilon_s \sigma\, T_s^4 \tag{3.2}$$

where

α_s = surface albedo,

ε_s = surface emissivity,

σ = Boltzmann constant, and

T_s = surface temperature.

At the surface, the short-wave balance is always positive, while the outgoing long-wave radiation generally exceeds incoming long-wave radiation. The model is constructed by parameterizing each of the components in the SEB in terms of routinely observed meteorological observations and site characteristics. A brief description of the SEB component parameterizations is presented below.

Incoming solar radiation at the surface is determined by using a variation of the Parameterization C model (Iqbal 1983). In this model, the solar radiation incident on top of the atmosphere is determined from earth-sun relationships and then adjusted via transmittance functions to account for atmospheric absorption and scattering. Separate transmittances are specified for (1) absorption due to (a) ozone, (b) water vapor, and (c) aerosols and for (2) scattering due to (a) Rayleigh particles (molecules) and

(b) aerosols. In addition, the model accounts for multiple reflections of solar radiation between the ground and the atmosphere, which significantly increase solar radiation when the surface albedo is high (e.g., deserts or snow cover). Along with data on location and time, the model requires data on (1) local atmospheric pressure; (2) surface albedo; (3) visibility; (4) precipitable water content, which is derived from upper-air data; and (5) ozone amount, which is estimated from latitudinal-seasonal averages. Attenuation due to cloud cover is estimated from the opaque and total cloud cover and cloud height by a semi-empirical model that was developed by Brown (1997) from an analysis of the National Solar Radiation Database (National Renewable Energy Laboratory 1993).

Net long-wave radiation at the surface is determined by using data on surface temperature, emissivity, near-surface temperature profiles, and humidity profiles. In particular, incoming long-wave radiation is estimated on the basis of a semi-empirical relationship developed from parameterizing long-wave radiation estimates from a detailed narrow-band radiation model. This relationship relies on data on the near-ground temperature profile, 10-m water vapor pressure, cloud fraction, and cloud height. Outgoing long-wave radiation is calculated directly from ground and foliage temperatures.

At the surface, the solar radiation and incoming long-wave radiation are balanced against the (1) sensible heat transfer, (2) latent heat transfer, (3) ground conduction heat transfer, and (4) outgoing long-wave radiation. To provide a physical, unified treatment valid under both daytime and nighttime conditions, SEBMET employs a two-layer canopy model that evaluates energy transfer components from both the ground and the vegetative layer. The model is formulated by writing separate energy-balance relationships for the ground and the vegetative canopy similar to Equations 3.1 and 3.2 and by parameterizing the energy transfer components in terms of available meteorological measurements and known vegetation and ground characteristics. The vegetative layer is characterized by the leaf area index and the bulk stomatal resistance, which is a measure of the latent heat transfer resistance. The key parameter is the bulk stomatal resistance, which embodies the physiological response of the vegetation to the ambient environment. In the SEBMET canopy model, this parameter is estimated by modeling the stomatal responses to (1) ambient temperature, (2) vapor pressure deficit, (3) solar radiation, and (4) moisture stress. Evaporation from the soil is considered by defining a moisture store in the soil layer that is reduced through evaporation and replenished by precipitation. The outgoing long-wave radiation is estimated directly from the canopy and ground temperatures and the canopy coverage percentage. Heat conduction into the ground is estimated by using a numerical, finite-difference algorithm that allows the dependence of soil properties and the insulating effect of overlying vegetation and snow to be explicitly treated. Such a scheme allows the ground temperature profile to be saved for use in pool evaporation calculations in the CASRAM emission rate model.

3.2.2.2 Inversion Height and Boundary Layer Height

The inversion height in convective condition is estimated with a one-dimensional model of the atmospheric boundary layer based on the Driedonks slab model (Driedonks 1982). In the Driedonks model, as in similar models, the surface turbulence fluxes u_* and H are integrated over time so the boundary layer evolves from an initial early morning height. The Driedonks model was chosen because of its comprehensive treatment of dynamics at the inversion, favorable comparison with field data, and ease of inclusion in the preprocessor.

In neutral and stable conditions, the boundary layer height is less well defined. Generally, the boundary layer height, at least in stable conditions, is taken to be the height at which surface-induced turbulence drops to a negligible value. Here, the diagnostic relations for stable conditions defined by Nieuwstadt (1981) and provided by the neutral limit ($h = 0.3u_*/f$, where f is the Coriolis force) are used, following the recommendations of Hanna and Paine (1989). (Hanna and Paine recommend that the neutral relation be used when L is greater than or equal to 100 and that Nieuwstadt's relation be used when L is more than zero but less than 100.)

3.2.3 Water Temperature for TIHWR Reaction Rates

As discussed in Section 3.3.3, water temperature has a significant influence on the reaction rates of water-reactive materials. In fact, the reaction rate of many materials roughly doubles for every 10°C increase in temperature. To account for this effect in our statistical hazardous materials analysis, we developed a database for water temperature as a function of location and Julian day. We investigated the following three sources of water temperature data.

1. *Great Lakes Buoys (GLBs).* Data were available from eight buoys scattered throughout the Great Lakes, whose reported temperatures yielded a multiyear average that was parameterized as a function of Julian day (Lesht and Brandner 1992).

2. *U.S. Geological Survey (USGS) Water Quality Network (WQN).* The USGS gathered data on stream water temperatures for periods of up to 30 years before 1990 at about 680 water stations (the WQN data). The data were for uneven durations and taken at uneven frequencies. In the best cases, monthly temperature values were recorded for a period of 20 years or more. For most stations, the day of the month and the time of day on which measurements were recorded varied, and about one month elapsed between measurements.

3. *National Oceanic and Atmospheric (NOAA) Ocean Harbor Buoys.* Data from a series of harbor buoys along the Atlantic and Pacific Coasts were recorded for years. Data from a representative set of locations were examined and found to substantively agree with the USGS data as a function of latitude. Therefore, the harbor buoy data were not specifically used for this study.

We selected a set of 35 WQN stations on the basis of several criteria. We wanted the network of stations to cover the United States evenly, or, if concentrated, to represent population centers. We needed data from a period of 20 years to permit meaningful climatological modeling. In actuality, while the target was about 240 temperature values, we chose stations that had recorded between about 150 and 450 values. With the addition of the 8 GLB stations, the total number of temperature stations we chose was 43. The locations of the temperature stations are shown in Figure 3.9.

We used a special parameterization of average GLB values by Julian day published by Lesht and Brandner (1992) for this study. For each WQN station or harbor buoy, the full set of values was fitted to the following equation:

$$T(J) = T_{avg} + (\Delta T)\sin\left(2\pi\frac{J - J_o}{365}\right). \tag{3.3}$$

The values of T_{avg}, ΔT, and J_o were fitted to all of the values. The GLBs were fitted with a six-parameter function given by Lesht and Brandner (1992). Because the formula has six adjustable constants and is somewhat detailed, it is not provided here; the original Lesht and Brandner (1992) article can be reviewed.

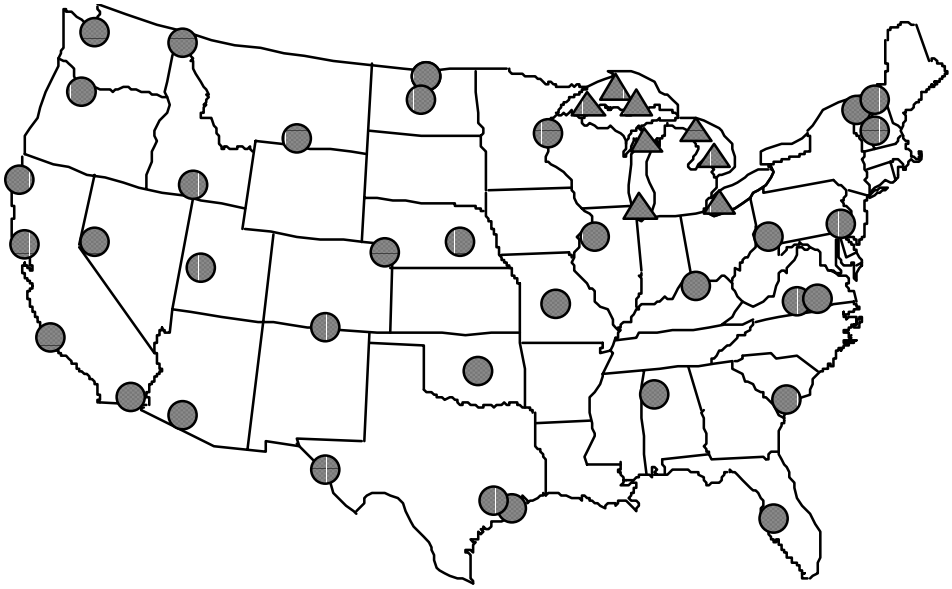

Figure 3.9 Water Quality Network Stations Used to Determine Variations of Average Water Temperature by Julian Day and Location (circles = 35 land-based sampling sites; triangles = 8 GLBs)

3.3 Emission Rate Characterization

3.3.1 Overview of Release Types

Materials are shipped as solids, ordinary liquids, compressed gases or liquefied gases. The emission rate of the material to the atmosphere largely depends on the shipment state. Because of their low volatility, solids typically exhibit low emission rates. Consequently, with few exceptions, non-water-reactive materials appearing on the TIH list are liquids and gases at atmospheric pressure. The remaining shipment states and water-reactive materials are illustrated in Figure 3.10 and discussed below.

Liquid materials are emitted to the atmosphere through pool evaporation (Figure 3.10a). The pool evaporation rate depends on many factors. For volatile liquids, the governing factors, in approximate order of importance, include (1) vapor pressure of the liquid, (2) available energy, (3) wind speed, and (4) atmospheric stability. In the case of low-volatility liquids (i.e., those characterized by low vapor pressure), meteorology replaces available energy in relative importance. Highly volatile liquids can evaporate very quickly (within minutes), cooling the pool in excess of 30°C below the ambient

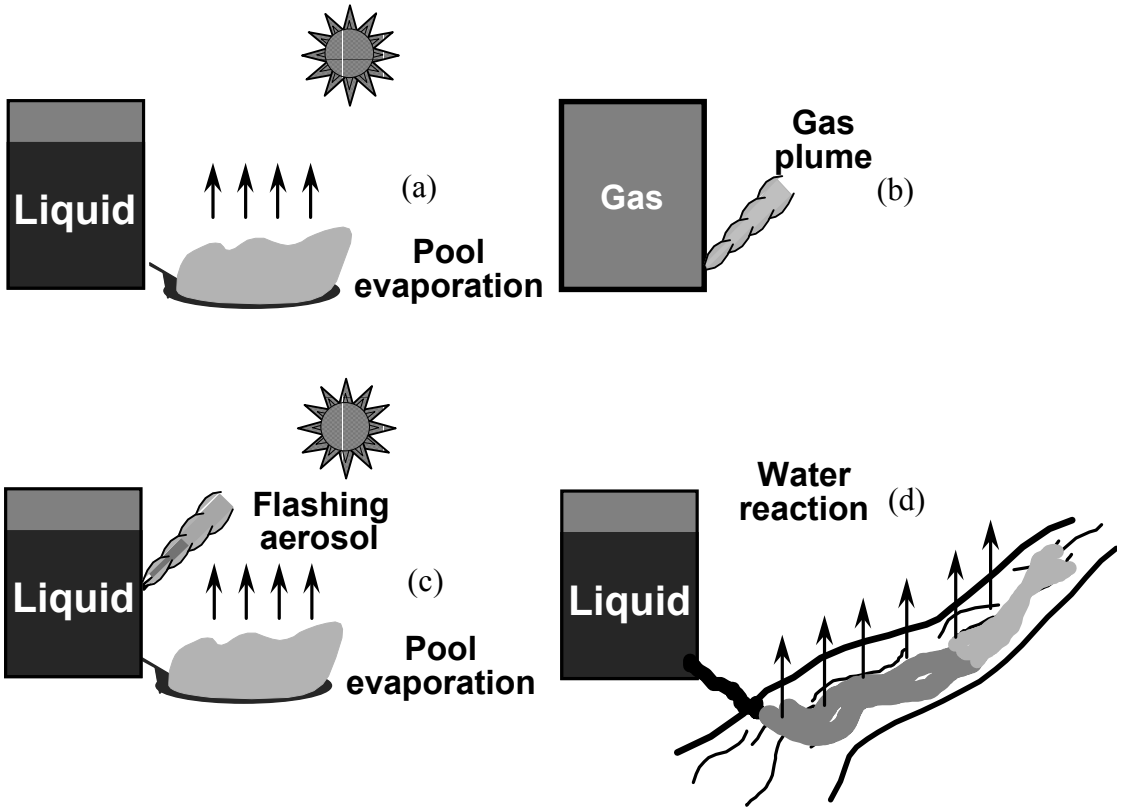

Figure 3.10 Important Source Types for Inhalation Risk Considered in the 2000ERG Analysis (a = ordinary liquids, b = compressed gases, c = liquefied gases, d = water-reactive materials)

temperature. In such cases, the evaporating material can actually freeze, thereby lowering the evaporation rate.

Compressed gases are released in a so-called blowdown process (Figure 3.10b). This process usually empties the container rapidly and, in the case of severe accidents, may result in an almost instantaneous release. All else being equal, release rates of compressed gases are many times faster than those of ordinary liquids. The exceptions are valve leaks and minor cracks, for which release rates may be very slow. For compressed gases, valve failures are the most common release mechanism for en route/nonaccident releases.

The most catastrophic form of release involves liquefied gases (Figure 3.10c). Here, the release is broken into two phases. In the initial phase, denoted as the flashing and entrainment phase, a fraction of the material (usually 0 to 30% of the total) is instantaneously vaporized upon exiting the vessel as a result of the sudden reduction in pressure. Because the material expands rapidly, much of the remaining liquid exiting the vessel is broken into tiny drops, forming an aerosol. The vapor typically entrains substantial quantities of this aerosol with the larger droplets quickly settling to the ground or "raining out." This aerosol usually evaporates quickly when exposed to air, cooling the vapor/air mixture to a point at which the density of the mixture can become considerably heavier than air. The liquid remaining on the ground or surrounding surfaces is then released through evaporation. Since the vapor pressures for such materials are usually well above atmospheric pressure, the evaporation phase is usually short, especially in comparison with the pool evaporation phase for materials that are liquids at atmospheric pressure. Because of the large quantities of material typically involved, release rates of liquefied gases are usually higher than those of liquids and compressed gases.

An additional class of materials discussed throughout this report and treated in the 2000ERG analysis is water-reactive materials. These materials release toxic gases to the atmosphere through the reaction of a parent chemical with water. Therefore, a water-way entry or an additional water exposure mechanism is required for them to become an inhalation risk problem. Although the release rate of the toxic by-product to the atmosphere depends primarily on chemical reactivity, many other factors also influence the reaction rate. For example, whether the parent chemical is heavier or lighter than water (solids and some liquids) will affect the mixing rate and therefore the reaction rate. Highly exothermic water reactions will result in faster reactions, more turbulent mixing of water with the chemical, and more rapid introduction of the TIHWR gas to the atmosphere. Rivers are generally more turbulent than some other bodies of water, thus enhancing mixing. Chemicals that spill into nonflowing water bodies also undergo turbulent mixing, but it results from other, generally weaker, mechanisms, such as turbulence produced by heat release in exothermic reactions or wave-generated turbulence due to wind. The reaction rates of these materials also depend rather strongly on water temperature and secondarily on water acidity.

3.3.2 CASRAM Emission Model and Its Application to the 2000ERG Analysis

The source component of CASRAM determines hazardous material release rates for each of the spill and/or vaporization scenarios described above. Information on the shipment, location, and meteorology are employed in the emission rate model to determine the amount of material spilled and the release rate. First the discharge fraction is estimated by using statistical distributions generated from analysis of HMIS database incidents, as discussed in Section 3.1.2. Then one or more physical models are employed to estimate chemical discharge rates and evaporation rates.

3.3.2.1 Assumptions Used to Develop Accident Scenarios

In developing the accident scenarios, the following assumptions were used:

- For accident-related releases from rail shipments (i.e., tank cars) involving a container breach (60% of total), the release rate of material from the container is regulated by the size of the hole, which is specified statistically according to hole size distributions presented by Raj and Turner (1993). Since no comparable data exist for highway transportation, the hole size distributions for highway bulk containers are set to those for tank car types having similar specifications (wall thickness, insulation). Total release amounts are limited to conform with discharge fraction distributions in the HMIS database by varying the location of the hole in the container.

- For en route/nonaccident incidents and for package freight accident-related incidents, release amounts are determined directly from the HMIS database release fraction distributions. For these incidents, the release is assumed to occur uniformly over a period of 15 min. This method overpredicts the impacts from slow leaks. However, this overprediction has little effect on PAD values, since slow vapor releases typically involve the release of small amounts of material and fall well below the 90-percentile level of protection cutoff.

- Liquids released from the container that are not flashed or entrained with the flashed liquid form a pool on the ground that expands and contracts in response to gravity-driven fluid flow and evaporation. For highway-related releases, 50% of spills are assumed to occur on paved surfaces. For rail releases, 25% of spills are assumed to occur on pavement or roadbed. All other spills are assumed to occur on natural surfaces characteristic of the accident locale. Ground temperature profiles to a depth of 1 m are provided in the preprocessed meteorological database.

- The discharge rate of water-reactive materials from their containers is varied so that 18%, 40%, 60%, and 95% of the total release amount is discharged in the first 5, 15, 30, and 60 min, respectively. The total release amounts are selected to conform with discharge fraction distributions in the HMIS database. The time-dependent emission

rate of the TIH by-product from the water is calculated from the container release rate and the reaction rate of the chemical with water.

- Except for the reaction of water-reactive materials to produce TIH by-products, chemical transformation is not considered.

- The temperature of the material upon release is taken as a weighted average of the air temperature and 290 K, with the exact weight depending on the container type.

3.3.2.2 Physical Considerations

Discharge from Tanks

In CASRAM, tanks that are punctured below the liquid line release their contents according to the Bernoulli equation (Perry et al. 1984); namely,

$$Q = c_o A_h \rho_l \left[2g\Delta h + 2\left(\frac{P_t - P_a}{\rho_l} \right) \right]^{\frac{1}{2}}, \tag{3.4}$$

where

Q = liquid release rate (kg/s),

c_o = discharge coefficient,

A_h = hole area (m^2),

ρ_l = liquid density (kg/m^3),

g = gravitational acceleration (9.81 m/s^2),

Δh = height of liquid above the hole (m),

P_t = tank pressure (Pa), and

P_a = atmospheric pressure (Pa).

In CASRAM, c_o is set to 0.6 for all releases.

Equation 3.4 is used to calculate the discharge rates from all bulk containers in CASRAM, where A_h is provided by the hole size distributions given by Raj and Turner (1993). If the material is a liquid, it forms a pool on the ground or pavement, which expands and contracts in response to gravity-driven fluid flow and evaporation. Liquefied gases, on the other hand, equilibrate to atmospheric pressure through flashing (explosive evaporation of a fraction of the released material). A fraction of the remaining

material is aerosolized and entrained in the flashed vapor, and the remaining material falls to the ground and evaporates.

Pool Evaporation

The release rate of material from an evaporating pool is represented such that

$$Q = A_p E_c, \tag{3.5}$$

where

A_p = pool area (m^2) and

E_c = evaporation rate from the pool ($kg/m^{2)}$.

Pool evaporation in CASRAM is determined by using a time-dependent, energy budget model that considers heat transfer to and from the pool via radiation, convection, conduction, and evaporation. Conductive heat flux from the ground is especially important and is often the dominant source of available energy, especially for very volatile liquids. Treating conduction correctly, especially the initial and boundary conditions, was a principal motivation in the development of the CASRAM evaporation model.

The energy budget of the pool is a balance between solar radiation S, incoming long-wave radiation L^+, outgoing long-wave radiation $\varepsilon_p \sigma T_p^4$, convective heat transfer H_p, latent heat transfer of water vapor from plant material λE_{wp}, conductive heat transfer to ground G_p, chemical evaporation rate $h_{fg} E_c$ (subscript p variables refer to pool-specific quantities), and energy storage mc_p (dT_p/dt). Therefore, the pool energy budget is

$$Q_p^* = H_p + \lambda E_{wp} + G_p + h_{fg} E_c + mc_p \frac{dT_p}{dt}, \tag{3.6}$$

where

m = liquid mass of pool (kg/m^2) and

c_p = specific heat of liquid ($kJ/[kg \times K]$)

and where Q_p^* is the net radiation given by

$$Q_p^* = (1 - \alpha_p) S + L^+ + \varepsilon_p \sigma T_p^4 \tag{3.7}$$

and G_p is the ground heat flux to the pool given by Fourier's law as

$$G_p = -k_g \left(\frac{dT}{dz} \right)_{z=0}. \tag{3.8}$$

In these relationships, ε_p is the pool emissivity, α_p is the pool albedo, and k_g is the ground or surface conductivity. The necessary transfer coefficients for evaporation are provided by a chemical property database and the preprocessed meteorological database discussed in the Section 3.2. In particular, the meteorological quantities of interest include aerodynamic resistances based on stability and wind speed, air temperature, incoming solar and long-wave radiation, and the initial ground temperature profile.

Compressed Gas Releases

In CASRAM, compressed gas releases are modeled by using semi-empirical blowdown relationships based on compressible-flow theory. Releases are assumed to be isentropic rather than isenthalpic. The isentropic assumption is that heat transfer to the vessel is negligible, which is a reasonable approximation for most accidental releases. The isenthalpic approximation, on the other hand, requires sufficient heat transfer to maintain isothermal conditions (assuming c_p is constant).

For compressed gas releases, the release rate is calculated on the basis of hole size, tank pressure, and gas density such that

$$Q = c_o A_h \left[P_t \rho_g \gamma \left(\frac{2}{\gamma+1} \right)^{\frac{\gamma+1}{\gamma-1}} \right]^{\frac{1}{2}}, \tag{3.9}$$

where γ is the specific heat ratio c_p/c_v. As in the case of liquid releases, c_0 is set to 0.6 for all releases.

Equation 3.9 is applicable until the tank pressure drops below a critical value, given as

$$P_r = \left(\frac{\gamma+1}{2} \right)^{\frac{\gamma}{\gamma-1}}, \tag{3.10}$$

where P_r is ratio of the tank pressure to atmospheric pressure. After this criterion is reached, the discharge rate is given by

$$Q = c_o A_h \left[P_t \rho_g \left(\frac{2\gamma}{\gamma-1} \right) \left(P_r^{-\frac{2}{\gamma}} - P_r^{-\frac{\gamma+1}{\gamma}} \right) \right]^{\frac{1}{2}}. \tag{3.11}$$

Calculations are conducted iteratively by adjusting the tank pressure and density at each time step with the isentropic assumption.

Liquefied Gas Releases

Liquefied gas releases are treated by first calculating the liquid release rate from the container given by Equation 3.4. As discussed previously, this material either flashes to vapor, is aerosolized and entrained with the vapor, or remains liquid and falls to the ground. This flash fraction f is given by

$$f = \frac{c_p(T_t - T_b)}{h_{fg}}, \tag{3.12}$$

where T_t is the tank temperature and T_b is the boiling point. This fraction of remaining material that is aerosolized and entrained into the flashed vapor is calculated by using empirical relationships based on the discharge kinetic energy of the two-phase mixture. Released material that does not flash to vapor or become entrained in the vapor clouds is deposited on the ground. Evaporation of the remaining material is then estimated by using the pool evaporation algorithms.

3.3.2.3 Water-Reactive Materials

For water-reactive materials, a different method is needed to estimate TIH emission rates to the atmosphere. Because of the myriad of water body types, reaction scenarios, and release mechanisms; the general lack of historical data on water entry releases; the inadequate characterizations of water body turbulence and mixing; and the lack of experimental data to validate sophisticated water reactivity models, treatment of all possible incident scenarios is not possible. It was therefore necessary to develop a simplified general approach for assessing the level of public protection required for each spill. This general framework will be expanded in future work, as new data on water reaction rates and accident scenarios become available.

The basic formula employed to compute the release rate of the TIHWR gas is

$$Q = M_O f_S \varepsilon C (1 - e^{-Ct}), \tag{3.13}$$

where

Q = release rate of TIHWR product (kg/s),

M_O = initial mass of parent chemical released into water,

f_S = maximum stoichiometric yield (kg TIHWR/kg parent chemical),

ε = efficiency factor for the reaction ($0 \le \varepsilon \le 1$), and

C = primary rate coefficient for water reaction (s^{-1}).

If the parent chemical is released over a significant period of time rather than suddenly, this formula yields values for ΔQ that result from the appropriate time decay for each $\Delta M(t)$ released.

Experimental data for ε or C in Equation 3.13 are very rare in the chemical literature. An extensive search of the literature at libraries and through on-line *Chemical Abstracts* yielded only qualitative descriptions of water reactivity for most of the TIHWR materials identified. Such descriptions allow only a crude estimate of either parameter, good to perhaps a level of 0.2 or 0.3 in a range from 0 to 1.0. Moreover, troubling inconsistencies in these qualitative descriptions were found in different literature sources. In several cases, the descriptions disagreed with the direct experience of at least one of the authors. We could not find any examples in which the deliberate release of a bulk chemical into a relatively large amount of water had been followed by the measurement of TIHWR production amounts.

Consequently, we conducted a modest series of direct experiments on 21 representative chemicals to shed light on classes of TIHWR chemicals. Of necessity, these experiments were small in scale and ignored important issues that would need to be addressed if results were to be scaled up to the size of transportation spills. Nevertheless, the experiments greatly increased the accuracy of estimates of ε. They also provided a direct measure of C, which is even harder to estimate from the qualitative descriptions.

On the basis of results from the experiments, we were able to delete about 10 chemicals from the TIHWR list, either because no reaction was observed or because the TIH gas that was released was readily reabsorbed into the water. This latter effect may not occur when large quantities are involved, and future experiments could show the net amount of TIHWR that would escape would require protective action. However, since TIHWR gas is absorbed so rapidly in small quantities, we expect that larger quantities would not pose great danger.

A review of literature on TIHWR chemicals showed that only two aspects of water quality seemed likely to influence their reactions in water: acidity and temperature. For a few chemicals, the presence of acidity was reported to increase the speed and degree of the reaction. However, the characterization of these effects was not well developed. Because of the poor characterization of these effects and the difficulty of obtaining water acidity data for natural water bodies, we did not attempt to account for water acidity variations in the 2000ERG analysis. The effect of temperature is substantially stronger than acidity, however. The reaction rate of many materials roughly doubles for every 10°C increase in temperature. Fortunately, the temperature of natural water bodies is well characterized by a network of water quality stations and buoys, as discussed in Section 3.2.3. The temperature dependence of the primary rate constant C was included in the analysis via the Arrhenius equation, written as

$$C = C_o \exp\left[-6610\left(\frac{1}{T_w} - \frac{1}{T_o}\right)\right], \tag{3.14}$$

where T_O = 20°C and T_W is water temperature determined by the procedures outlined in Section 3.2.3. The chemical-specific constant C_O was determined experimentally. In applying this relationship, the rate constant C for a given hypothetical spill was specified by finding T_W on the Julian day of the simulated accident at the nearest WQN or GLB station. Then the Arrhenius formula was applied to the rate constant listed as the constant C_O in Table D.1 in Appendix D.

3.4 Analysis of Atmospheric Dispersion

Hazardous material releases that occur during transportation accidents are typically at ground level. The ground-level concentration that occurs downwind of the release site decreases with distance as the plume (or puff in the case of instantaneous releases) spreads horizontally and vertically. In the dispersion modeling phase of the problem, the emission rate and the prevailing meteorology are employed to estimate the chemical concentration field downwind of the release point. For this study, the maximum concentration, which occurs on the plume centerline, is of primary interest, since it governs the required PADs for a given material.

For passive dispersion (i.e., dispersion in which buoyancy of the plume is insignificant), downwind concentrations are linearly related to (1) the release rate if the release is continuous or (2) the release amount of the release is instantaneous. The dependence of meteorology on dispersion is modeled by evaluating the effects of wind, temperature, cloud cover, solar radiation, and other factors on critical turbulence and structural parameters of the atmospheric boundary layer. The key parameters include wind speed, friction velocity, surface heat flux, and boundary layer or inversion height.

The dispersion method used in the 2000ERG analysis differs substantially from the method that was used in preparing the 1996 ERG. First, for the later analysis, we adopted the vertical dispersion model of Brown (1997), which is applicable for calculating ground-level concentrations from near-ground releases. This passive dispersion model is considerably more sophisticated than the one employed in the 1996 analysis and results in predictions that are significantly different on an individual (case-by-case) basis. However, on a total basis (when the entire spectrum of incidents considered in the analysis of PAD values is considered), these differences are relatively minor and do not change the PAD values by more than 10%. A second significant difference in the two methods involves the incorporation of a dense gas dispersion module into the CASRAM framework for the 2000ERG analysis. The dense gas model is employed mainly for those liquefied gas releases in which cooling of the plume and aerosol entrainment increase the plume density to the point where the passive dispersion assumption is no longer valid. For many liquefied gases, especially those that are highly toxic, dense gas dispersion models provide results very similar to those from passive gas dispersion models in terms of PADs. For a narrow class of less toxic liquefied gases such as ammonia, implementation of the dense gas model does have a more substantial effect.

3.4.1 Overview of Atmospheric Dispersion

3.4.1.1 Diurnal Aspects of Plume Dispersion

The physical processes governing the development and maintenance of the atmospheric boundary layer (ABL) are very different during day and night, leading to boundary layers with extremely different sizes and characters. These marked differences substantially influence the ability of the ABL to disperse pollutants released near the ground, thereby giving rise to the pronounced differences in downwind concentrations and therefore in PAD values appearing in the Table. This section briefly describes the characteristics that distinguish the daytime and nighttime ABLs and elucidates how these variations lead to the differences in PAD values between the two cases.

The unstable or convective boundary layer (CBL), typical of daytime conditions, is shown in Figure 3.11a. The boundary layer structure is a result of the surface heating caused by solar radiation. This heating destabilizes the lower layers of the ABL, producing large convective cells. These convective cells extend vertically to the lowest temperature inversion, and they efficiently transport heat, momentum, and any material contaminants released into the atmosphere. As the day progresses, the temperature inversion marking the top of the boundary layer rises from near the ground to between 0.5 and 4 km above the surface as a result of the entrainment of stably stratified air above the inversion into the cooler air of the boundary layer below.

An example of a dispersing plume in a typical CBL is pictured in Figure 3.11b. Experimental observations, most notably those of Willis and Deardorff (1976), have indicated that vigorous convection, which typifies the CBL, results in a “rising centerline” phenomenon. In this process, energetic thermals lift the plume or cloud off the ground faster than it disperses downward. This consequence of dispersion in a fully convective boundary layer is primarily responsible for the rapid decay of material concentrations downwind from ground-level sources when the release occurs in the middle of the day.

In the absence of solar heating, the nighttime ABL structure is driven by cooling at the surface as heat is radiated to space. This situation leads to the development of a stably stratified boundary layer (SBL), which is typically much shallower and less energetic than its unstable counterpart, as illustrated in Figure 3.12a. The surface cooling strongly stratifies the low-level air, thereby creating a tenuous balance between the turbulence produced by wind shear and turbulent energy dissipation. The rapid dissipation of turbulent energy greatly limits the vertical eddy size and restricts vertical mixing.

Dispersion in a typical SBL is pictured in Figure 3.12b. The vertical stability and shallow depth profoundly affect dispersion processes by confining material contaminants

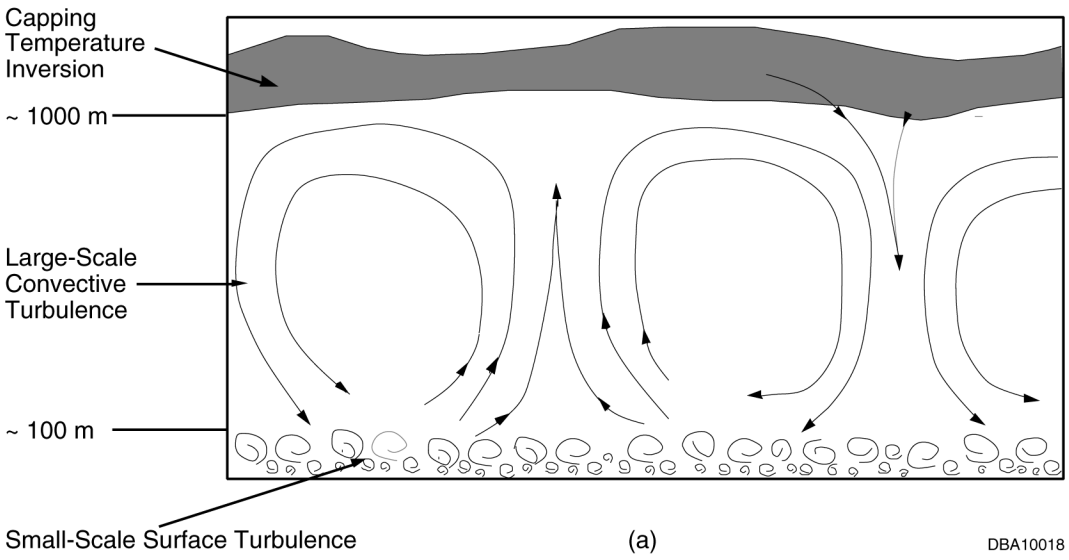

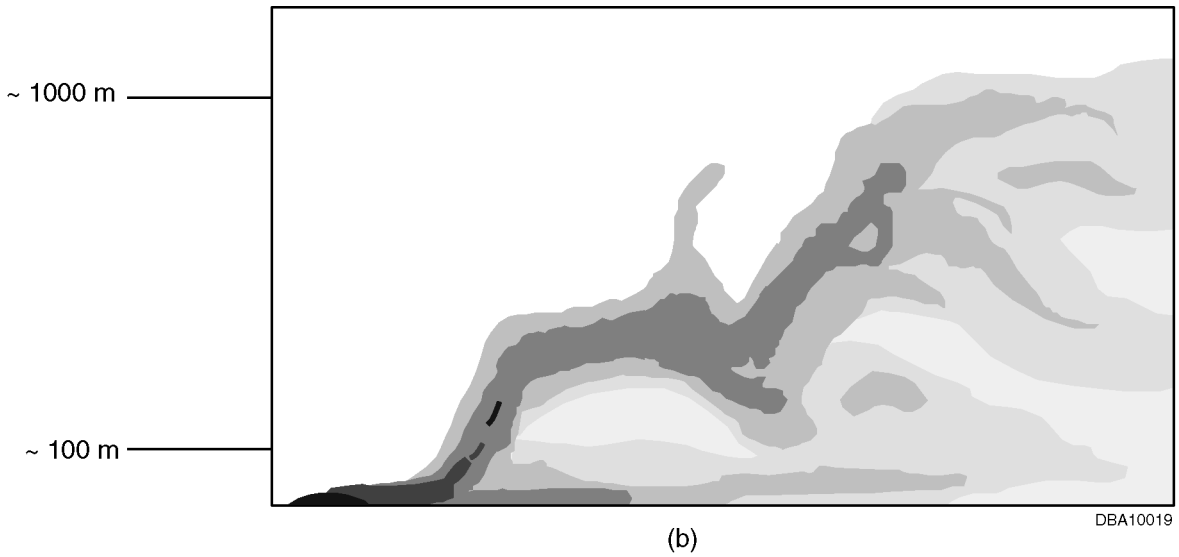

Figure 3.11 Typical Daytime Convective Boundary Layer Showing (a) an Instantaneous Wind Field and (b) an Instantaneous Material Concentration Field from a Ground-Level Release (characteristic height of about 1,000 m for the boundary layer and about 100 m for the surface layer provided for reference)

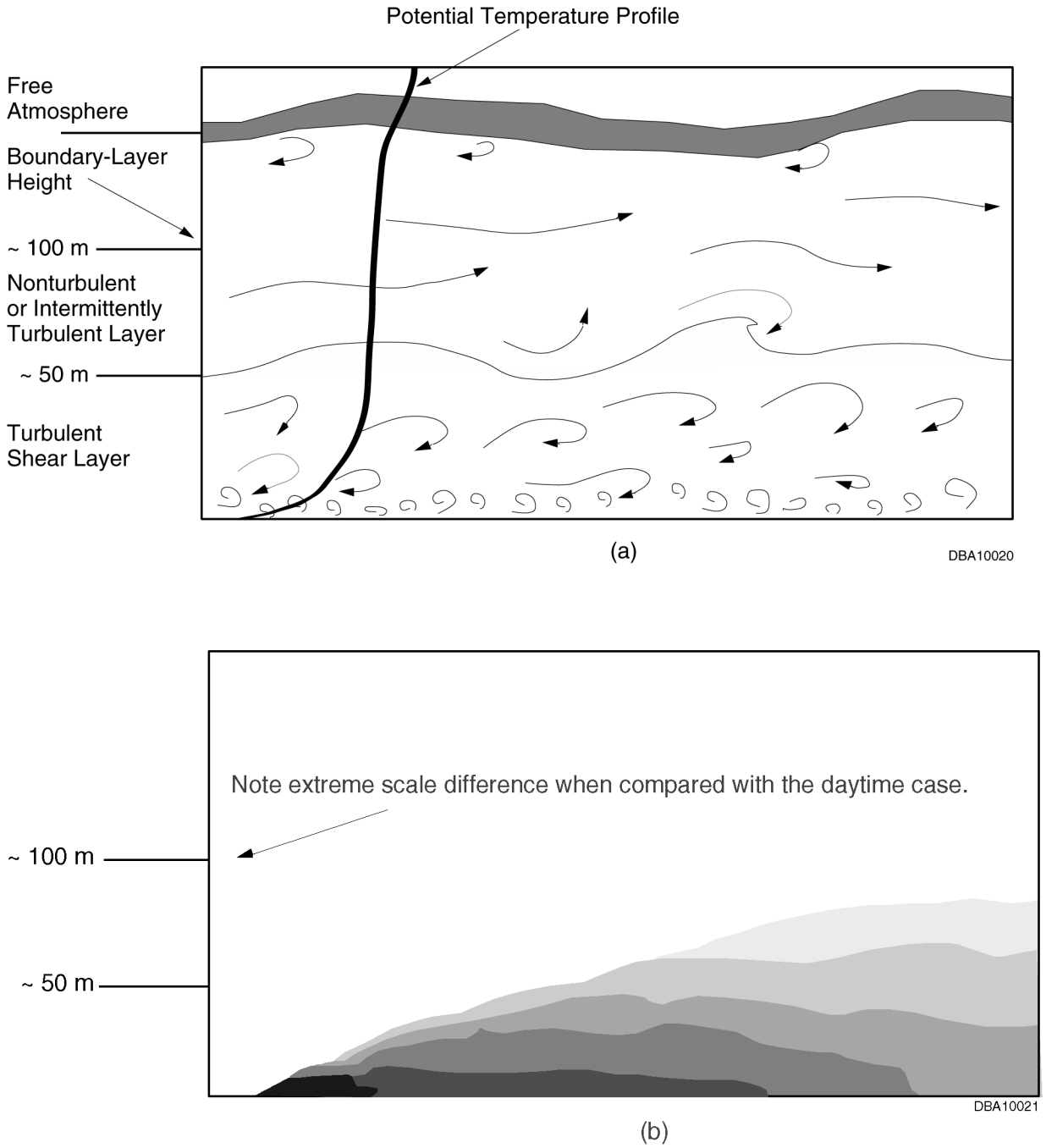

Figure 3.12 Typical Nighttime Stable Boundary Layer Showing (a) an Instantaneous Wind Field and (b) an Instantaneous Material Concentration Field from a Ground-Level Release (characteristic height of about 50 m for the surface shear layer and about 100 m for the boundary layer provided for reference)

to a thin layer near the ground. In very stable conditions, such as those represented in the 90-percentile level of safe distance distributions, the SBL is usually less than 50 m deep. When a contaminant is released into the SBL, it diffuses to its maximum vertical extent in a relatively a short distance, forcing most of the dispersion to occur two-dimensionally along the ground. This plume confinement allows comparatively high concentrations to be observed near the surface at considerable distances from the release site, leading to the PADs that are further from the source than are necessary for daytime incidents.

3.4.1.2 Effects of Dense Gas on Plume Dispersion

The discussion of atmospheric dispersion to this point has been confined to passive dispersion (i.e., cases in which the density of the ambient plume does not affect its dispersion). However, in many cases of practical interest, the effect of a high density (relative to air) of the hazardous chemical discharge becomes important in considering impacts within 1 to 2 km of the release point. So-called dense gas effects result not only from the properties of the material released but also from the methods of storage and the conditions of the release. Most cases of interest have focused on combustibles or toxic compounds that have boiling points below ambient temperature. These compounds are commonly transported or stored as liquids and then maintained in liquid phase (1) at or near their saturation temperature at atmospheric pressure by refrigeration and insulation (i.e., refrigerated liquid) or (2) at ambient temperature by pressurization (i.e., pressurized liquid or liquefied gas). For transportation incidents, cases that could lead to significant dense gas effects fall into one or more of the following broad categories:

- Chemicals with a high molecular weight when compared with air (e.g., chlorine, arsine) coupled with a large release quantity or high release rate (i.e., >1 kg/s);

- Refrigerated chemicals with a relatively low molecular weight when their temperature upon release is cold relative to the ambient temperature (e.g., a cold methane release evolving from the boiling of refrigerated liquefied natural gas);

- Pressurized liquids containing chemicals with a low to moderate molecular weight that, although they are less dense than air at their boiling point, cool rapidly and entrain aerosol generated in the release process, thereby creating a denser-than-air plume; and

- Chemicals that undergo molecular association (hydrogen fluoride [HF]) and/or transform to secondary hazardous compounds because of their ambient water-vapor reactivity (e.g., sulfur trioxide [SO_3]/oleum, nitrogen tetroxide [N_2O_4]). (These are not necessarily the same group of compounds that are water-reactive as defined in this report.)

Several major effects can be observed during the dispersion of a ground-level, dense gas cloud that do not occur during the dispersion of a neutrally buoyant cloud. One is that there is less vertical turbulent mixing between the dense gas cloud and the ambient atmosphere because of the stable density stratification of the cloud relative to the

surrounding ambient air. Another is the presence of gravity-induced flow resulting from horizontal density gradients. These two effects result in a shallower and much wider cloud than the cloud that results from an analogous neutral density release. In addition, the movement of the dense gas cloud on uneven terrain can follow the downhill slope independent of the wind direction, and the cloud can become trapped in valleys or low spots. The magnitude of these dense gas effects depends on the size of the release, local meteorological conditions, and the physical properties of the chemical release.

3.4.2 CASRAM Dispersion Model

3.4.2.1 Passive Dispersion

Like many other dispersion models, CASRAM separates the dispersion calculation into two components: horizontal dispersion and vertical dispersion. In CASRAM, vertical turbulent dispersion is treated with a Lagrangian-integral model parameterized in terms of mean plume height, average advection velocity, and a dimensionless travel time. These parameters are expressed as integral equations written in terms of plume travel time and atmospheric boundary layer parameters. Continuous releases are treated as plumes, and instantaneous releases are treated as puffs. Horizontal turbulent dispersion is represented via Gaussian relationships that are parameterized in terms of the Lagrangian time scale and lateral wind direction fluctuations. Plume calculations are straight line in nature, since terrain effects are not currently considered in CASRAM.

The concentration relationship for continuous plume releases from point sources is represented in terms of the crosswind-integrated concentration (CWIC), chemical mass release rate Q, and traditional Gaussian expression for the horizontal plume spread. The ground-level concentration distribution is computed as follows:

$$C(x,y,z=0)=\frac{Q\hat{C}_y(x,z=0)}{\sqrt{2\pi}\sigma_y}\exp\left[-\left(\frac{y}{\sqrt{2}\sigma_y}\right)^2\right], \tag{3.15}$$

where

$\hat{C}_y$ = CWIC normalized by the release rate,

σ_y = lateral plume spread, and

y = lateral distance from the plume centerline.

For time-variant evaporative emissions, the release rate is taken to be the average over the exposure time corresponding with the toxicological value.

For releases with finite width, corresponding to large pools releases or dense gas releases as they become passive, the following expression is used:

$$C(x,y,z=0) = Q\hat{C}_y(x,z=0)\left(erf\left[\frac{y_o - y}{\sqrt{2}\sigma_y}\right] + erf\left[\frac{y_o + y}{\sqrt{2}\sigma_y}\right]\right). \quad (3.16)$$

Peak concentration averages resulting from instantaneous releases are calculated according to the relationship

$$C(x,y,z=0) = \frac{M\hat{C}_y(x,z=0)}{\sqrt{2\pi}\sigma_y T}\text{erf}\left[\frac{\text{U}}{2\sqrt{2}\sigma_y}\text{T}\right]\exp\left[-\left(\frac{y}{\sqrt{2}\sigma_y}\right)^2\right], \quad (3.17)$$

where

M = total release amount,

T = averaging time, and

U = 10-m wind speed.

The subsections below first present the methodology for determining vertical dispersion (i.e., for determining C_y as a function of downwind distance). They then discuss the determination of σ_y, thus providing horizontal dispersion.

Vertical Dispersion

This discussion of the vertical dispersion model begins with a review of the surface-layer, similarity-based model of van Ulden (1978), since our approach represents a natural extension of this model. The van Ulden approach centered around writing an exact solution of the advection-diffusion equation. When written in terms of the CWIC form and neglecting stream-wise diffusion, it reads as follows:

$$U(z)\frac{\partial C_y}{\partial z} = \frac{\partial}{\partial z}\left[K_z(z)\frac{\partial C_y}{\partial z}\right], \quad (3.18)$$

where K_z is the vertical diffusivity for a scalar. The solution van Ulden advances is written in terms of the mean plume height $\bar{z}$, the average plume advection velocity $\overline{U_p}$, and the power-law wind speed coefficient m and diffusivity coefficient n. The coefficients m and n are defined such that

$$U(z) = u_o z^m \quad (3.19)$$

and

$$K_z(z) = k_o z^n , \tag{3.20}$$

where u_o and k_o are constants representing the wind speed and diffusivity at 1 m. From the early work of Roberts (1923), it is well known that the advection-diffusion equation subject to the above power-law relationships yields an exact solution (see Calder 1949). The work of van Ulden (1978) extends this analysis by using the power-law coefficients to determine the concentration profile shape *a priori* (i.e., from the Roberts analysis) and then formulates integral relationships for the mean plume height and average advection velocity in terms of the more physically correct similarity functions for wind speed and diffusivity. The van Ulden (1978) solution reads as follows:

$$\hat{C}_y(x,z) = \frac{A}{\bar{z}\overline{U_p}} \exp\left[-\left(\frac{Bz}{\bar{z}} \right)^s \right], \tag{3.21}$$

where

$$A = \frac{s\Gamma(2/s)}{\Gamma(1/s)^2}, \tag{3.22}$$

$$B = \frac{\Gamma(2/s)}{\Gamma(1/s)}, \tag{3.23}$$

and s is a shape parameter given by $1 - m - n$. In Equations 3.22 and 3.23, Γ represents the gamma function.

In applying this model, van Ulden (1978) parameterized the mean plume height and average advection velocity by using surface-layer similarity functions for wind speed and diffusivity. In a subsequent study, Gryning et al. (1983) extended this analysis by adding a sophisticated relationship to determine the shape parameter s as a function of stability and downwind distance. The relationships for s were determined through analysis of numerical solutions for the advection-diffusion equation for a wide range of conditions. In a detailed model-data comparison that used CWIC data from the Prairie Grass experiments (Barad 1958), Gyning and colleagues demonstrated the utility of the Lagrangian empirical model in representing the concentration profile as well as in estimating ground-level concentrations. This model provided an excellent description of dispersion in the surface layer. However, its application is limited to dispersion problems in which the plume is mainly confined to the surface layer. When the plume rises above the surface layer, the concentration profile given by Equation 3.21 as well as the similarity relationships for $\bar{z}$ and $\overline{U_p}$ become invalid. For problems of practical interest, this rather severe constraint on the use of Equation 3.21 strongly limits the applicability of the model for problems of practical interest.

Brown (1997) modified the original van Ulden work to correct this limitation. In this revised formulation, the normalized ground-level concentration is expressed as

$$\hat{C}_y(x,z=0) = \frac{A'(\tilde{s})F(x;u_*,z_i,H_s)}{z_u\overline{U_p}} \ , \tag{3.24}$$

where z_u is defined such that

$$U(z_u) = \overline{U_p} \ , \tag{3.25}$$

and

$$A'(\tilde{s}) = \frac{1.6\,\tilde{s}\,\Gamma(2/\tilde{s})}{\Gamma(1/\tilde{s})^2} \ . \tag{3.26}$$

Here, A' takes the same functional form as A in van Ulden's model, except that it is multiplied by 1.6 to account for the ratio of $\overline{z}$ to z_u and depends on a modified shape parameter denoted as $\tilde{s}$.

The main departure of this approach from the models of van Ulden and Gryning et al. is in the boundary-layer function F. This function is added to treat dispersion within the greater ABL outside the surface layer. As previously noted, the van Ulden model was developed by using the quasi-exponential concentration profile. For surface-layer dispersion, this assumed form for the concentration profile adequately represents the concentration profiles observed in field studies, most notably the Prairie Grass experiments. However, once the plume is influenced by boundary-layer effects outside of the surface layer, the concentration profiles depart significantly from the exponential form. In unstable conditions, this departure is particularly pronounced, since the plume centerline actually lifts off the ground, creating a maximum concentration aloft. In stable conditions, the opposite effect is observed, in which the concentration profile is flattened as a result of the rapid decrease in turbulent energy with height. The transition function F allows us to adapt this methodology, which was originally developed to model surface-layer dispersion, to treat dispersion throughout the entire ABL.

Brown (1997) developed relationships for z_u, $\tilde{s}$, and F by using a parametric analysis of a Langevin-equation Monte Carlo dispersion model validated with data from field and laboratory experiments. In applying the CASRAM vertical dispersion model, $\tilde{s}$ is a function of meteorology and therefore does not vary with distance, and F is represented as a function of travel time and meteorology. The heart of the calculation lies in z_u, which is calculated by using integral relationships represented as a function of travel time. Numerical integration of this relationship provides z_u as a function of downwind

distance, which, together with $\tilde{s}$ and *F,* allows the evaluation of Equation 3.24 and ultimately Equation 3.15, 3.16, or 3.17.

Horizontal Dispersion

Under horizontal homogeneous conditions, the Gaussian model correctly represents lateral concentration distributions. In CASRAM, the lateral spread from nonbuoyant releases can be related to the standard deviation of the horizontal wind fluctuations and is determined by using relationships originally proposed by Draxler (1976). Here, σ_y is given by

$$\sigma_y = \sigma_v f_y\left(\frac{t}{T_d}\right), \tag{3.27}$$

where

σ_v = standard deviation of transverse velocity,

t = transit time (estimated by using wind speed at 2 m and distance),

T_d = dispersion time scale related to the Lagrangian time scale, and

f_y = a nondimensional function of travel time.

The empirical form of f_y is estimated through evaluating field data. Several forms of f_y have been proposed (Irwin 1983; Gryning and Lyck 1984), but the empirical expression that provides the best overall fit with available field data is the form proposed by Draxler (1976). His function is given by

$$f_y = \frac{1}{1 + 0.9\sqrt{t/T_d}}. \tag{3.28}$$

For surface releases, a T_d of 300 s is used for unstable conditions and a maximum of 300 s or 0.001 t^2 s is used for stable conditions. The appeal of Draxler's relation is that it is developed from diffusion data from many experiments and that it is consistent with Taylor's limit for both small ($\sigma_y \sim t$) and large ($\sigma_y \sim t^{1/2}$) travel times (Taylor 1921).

Equation 3.27 requires the standard deviation of transverse velocity σ_v. In the absence of observational data, σ_v is determined by using the interpolation equation of Panofsky et al. (1977)

$$\sigma_v = u_*\left(12 - 0.5\frac{z_i}{L}\right)^{1/3} \tag{3.29}$$

during unstable conditions and the proportionality relation of Panofsky and Dutton (1984)

$$\sigma_v = 1.92\, u_* \tag{3.30}$$

during stable conditions.

In very stable conditions, Equation 3.30 fails to adequately represent σ_v, since wind speed and friction velocity become very small. For instance, if the friction velocity is about 0.015 m/s, indicative of a wind speed of about 0.5 m/s with $z_o = 0.1$ m on a clear night, Equation 3.30 predicts $\sigma_v = 0.03$ m/s. One kilometer from the source, this value of σ_v yields $\sigma_y = 36$ m from Equation 3.27. Considering the 2,000-s travel time, such a narrow plume width is not realistic when the meandering nature of stable boundary layer flows is considered. To overcome this problem, we assign a minimum value of 0.15 m/s for σ_v on the basis of observations presented by Hanna and Chang (1992).

3.4.2.2 Dense Gas Dispersion

Early in development of CASRAM, consideration was given to the issue of treating or not treating dense gas effects. Our analysis at that time showed that although dense gas effects are indeed important for large releases of certain liquefied gases, the effects are less important than other factors in the overall analysis (meteorology, release amount and rate, etc.) for hazard zone prediction. Since that original unpublished work was done, several dense gas algorithms have been found to perform well when compared with available experimental data. Also, because dense gas submodels are now included in more than 100 models applicable to hazardous materials releases, CASRAM's omission of dense gas effects has been increasingly identified as a significant shortcoming of the model, thus blocking its broader acceptance in the scientific community.

To address these concerns, a dense gas algorithm was added to the CASRAM methodology as part of the 2000ERG study after a detailed review of available dense gas algorithms models. The review identified five dense gas models that were well documented and would be applicable within the CASRAM framework: DEGADIS (Havens 1988), HEGADAS (Post 1994), SLAB (Ermak 1990), SCIPUFF (Defense Threat Reduction Agency 1999), and TSCREEN (U.S. Environmental Protection Agency [EPA] 1992).

The Britter & McQuaid Workbook dense gas nomogram formulation incorporated in the TSCREEN model was eliminated from further consideration because of the difficulty of incorporating its form (i.e., nomogram structure) into an integral model such as CASRAM. Although the SLAB model has some similarity parameterizations consistent with integral models, the shallow-layer approach adopted for SLAB did not allow a clean interface with the integral CASRAM passive gas formulation. The turbulent diffusion in SCIPUFF is based on a turbulence closure scheme. Also the model incorporates a concentration fluctuation variance equation upon which the formulations for mean flow

dynamics for negatively buoyant dense gas are based. Although this approach is fundamentally consistent with the stochastic integral framework upon which CASRAM is based, its treatment of turbulence and description of dispersion through a second order closure approach scheme are not consistent.

The remaining models, DEGADIS and HEGADAS, have very similar origins and formulations as well as performance with field data. Both can also be easily adapted into the current CASRAM formulation. The model incorporated into CASRAM at this time, as discussed in the section below, relies heavily on the empirical entrainment parameterizations within the DEGADIS formulation. The HEGADAS model is similar in nature but is currently being revised, partially on the basis of extensive field data collected in the recent PERF-supported kit fox studies. Future modifications to the CASRAM dense gas dispersion model may involve incorporation of the HEGADAS formulation.

Like the passive gas dispersion model used in CASRAM, the dense gas algorithm is integral in nature. The initial conditions are specified by the vapor release rate Q_v and aerosol release rate Q_a from the container, which are calculated from the CASRAM emission rate model. The first step is evaluating the volumetric flow rate of vapor exiting the container $\dot{V}_{sv}$, which is given by

$$\dot{V}_{sv} = \frac{Q_v}{\rho_v}, \tag{3.31}$$

where ρ_v is the density of the chemical vapor at the boiling point. The initial volumetric flow rate of the cloud $\dot{V}_{ci}$ is taken as

$$\dot{V}_{ci} = (1 + \beta_{ei})\dot{V}_{sv}, \tag{3.32}$$

where β_{ei} is the entrainment parameter at the source taken as 2. This is a rough estimate that depends on many factors. However, the model results at distances more than 10 to 20 m from the source are not sensitive to β_{ei}.

The initial cloud is assumed to have a flat, cylindrical shape (rectangular in two dimensions) with a width of $2r_i$ and height h_i, where $r_i = h_i$. To estimate the cloud dimensions from the volumetric flow rate, one must solve the relationship

$$h_{ci} = \frac{\dot{V}_{ci}}{2\overline{U_p} r_i}, \tag{3.33}$$

where

$$\overline{U_p} = u(z = 0.6h_{ci}). \tag{3.34}$$

The solution of Equations 3.33 and 3.34 are necessarily iterative and subject to the constraint that h_{ci} is more than 1.5 m.

The initial cloud density is then defined in terms of the sum of the mass flow rates of the "flashed" vapor and aerosol plus the entrained air as

$$\rho_{ci} = \frac{Q_v + Q_a + \beta_{ei}\dot{V}_v\rho_a}{\dot{V}_{ci}}, \tag{3.35}$$

where the last term on the right side of the numerator accounts for the mass of air initially entrained into the plume.

After release, the cloud spreads horizontally under the influence of its negative buoyancy while it grows vertically through entrainment of air from above. Note that dense gas plumes are marked by a much higher horizontal growth rate than vertical growth rate. The horizontal gravity spread is assumed to depend on the cloud advection speed and Richardson number for continuous releases and is computed in a form equivalent to the model of Raj (1985) such that

$$\frac{dr}{dx} = \frac{\beta_e u_*}{\overline{U_p}}\sqrt{Ri_*}\ . \tag{3.36}$$

Here, β_e is an entrainment parameter taken as 1.15 and $Ri*$ is the local cloud Richardson number given by

$$Ri_* = \frac{gh_c(\rho_c - \rho_a)}{\rho_a u_*^2}. \tag{3.37}$$

Vertical cloud growth is governed by vertical entrainment of air into the cloud, which can be conveniently defined in terms of cloud advection speed and entrainment velocity v_e in the integral equation

$$\frac{dh_c}{dx} = \frac{v_e}{\overline{U_p}}\quad , \tag{3.38}$$

where the vertical entrainment velocity is as used in the DEGADIS model; namely,

$$v_e = \frac{0.4u_*}{0.88 + 0.099Ri_*^{1.04}}\ . \tag{3.39}$$

Equations 3.36 and 3.38 make up a coupled set of differential equations that are solved at successive points downwind of the source. The solution proceeds until the

critical Richardson number *Ri* is less than 50. This critical Richardson number is defined differently than the local cloud Richardson number and is given by

$$Ri_c = \frac{U(h_c)(\rho_c - \rho_a) g h_c}{\rho_a u_*^3}. \tag{3.40}$$

After this Richardson number criterion is met, we initialize the passive gas dispersion model by matching the cloud height and assuming a uniform concentration across the width of the cloud of *2r*. Therefore, the parameter y_o in Equation 3.16 is set to *r*.